Propagators and scattering of electromagnetic waves in planar bianisotropic slabs - an application to absorbers and frequency selective structures

Andersson, Michael

2013

CODEN:LUTEDX/(TEAT-7225)/1-31/(2013)

Propagators and scattering of electromagnetic waves in planar bianisotropic slabs — an application to absorbers and frequency selective structures

Michael Andersson

Electromagnetic Theory
Department of Electrical and Information Technology
Lund University
Sweden

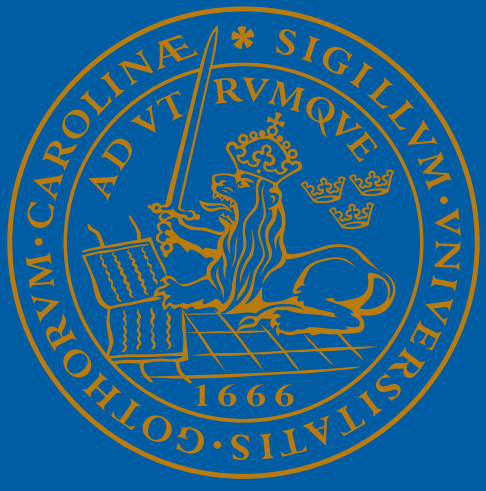

Michael Andersson
michael.andersson@gknaerospace.com

Radomes & Antennas
GKN Aerospace Applied Composites
Box 13070
SE-580 13 Linköping
Sweden

Editor: Gerhard Kristensson

Abstract

The concept of propagators for solving scattering problems in planar geometries has been generalized to accommodate thin homogeneous, in general anisotropic, resistive sheets embedded in supporting slabs, by the usage of a well known approximate impedance boundary condition. The slabs can be arbitrary linear materials *i.e.*, bianisotropic materials, and applications of the method to the analysis of single and multilayer absorbers *i.e.*, Salisbury and Jaumann absorbers are given. The generalization of the propagator method also handles the problem with an arbitrary number of metallic sheets consisting of resistive patch elements embedded in supporting linear, bianisotropic slabs. The solution of both the case of finite number of patch elements and the case where the elements are periodically arranged, is shown by the use of the Galerkin method. Numerical examples, where comparison to data presented in the literature as well as measured data, are shown in the paper.

1 Introduction

Wave propagation in planar geometries is a classical canonical scattering problem well used in science and technical applications for decades, see *e.g.*, [2, 5, 20, 22, 32, 33].

The foundation of the theory presented in this paper is the concept of propagators, which basically are mappings that relates the total transversal fields between points in space. The propagators provide a systematic approach to the analysis of solutions to complicated scattering problems, and propagators have been used for decades in *e.g.*, the theory of quantum mechanics [1]. There are, however, few publications on propagators in connection to electromagnetic problems despite the fact that the propagator method has similarities with the vector generalization of the transmission line theory [7, 27].

This paper presents a generalization of the theory of the propagator method presented in [29] to thin, homogeneous, in general anisotropic, resistive sheets. It is shown that the impedance boundary condition can be imposed into the concept of propagators formulated for handling one or several homogeneous resistive sheets imbedded in supporting slabs, where the materials in the slabs can be arbitrary linear materials, *i.e.*, bianisotropic materials.

The theory presented in [21] provides a method for solving scattering problems in planar geometries with an arbitrary number of metallic sheets consisting of aperture or patch type elements imbedded in supporting linear bianisotropic slabs. This paper extends the theory in [21] by considering lossy patch type elements by the usage of the above mentioned impedance boundary condition. The perfect conducting case reported in [21] is shown being a special case of the lossy case.

An important application of the theory presented in this paper is on the design of layered structures consisting of thin resistive sheets *i.e.*, radar absorbing materials (RAM). Absorbers can be constructed by placing one or several resistive sheets in a stratified structure. The classical Salisbury screen is the simplest design which consists of a single resistive sheet placed $\lambda/4$ in front of a perfectly conducting ground

plane (PEC backing), see *e.g.*, [3, 13, 23–25]. The bandwidth of the Salisbury screen is relatively small and can be extended by adding more resistive sheets spaced by suitable dielectrics approximately $\lambda/4$ apart. These multilayer absorbers are usually referred to as Jaumann absorbers, see *e.g.*, [4, 10, 11, 17, 23–25]. Another important application of the theory in this paper is the frequency selective surface (FSS) [23] *i.e.*, sheets with metallic scatterers arranged in a periodic pattern embedded into the structure. If the FSS is made of lossy elements it has been found that it is possible to modify and improve the absorbing performances of RAM further, [8, 16, 17, 23–25, 30]. Absorbers that contain sheets with resistive elements arranged in a periodic pattern are referred to as circuit analog absorbers (CAA), briefly because they contain resistive as well as reactive components [23]. The main advantage with the CAA structures is that it is possible to further improve the bandwidth with less cost in thickness compared to the classical Jaumann absorbers.

Furthermore, periodic structures can be designed to absorb in certain frequency bands while being transparent in others and those structures are termed as rasorbers [24]. Rasorbers are applicable in *e.g.*, radome applications where a protective structure for an antenna is needed. Specifically, stealth radomes are used in low observable applications [23]. Stealth radomes in principle reflect power from hostile radiation outside the antenna frequency band in the desired directions. In applications where it is difficult to reflect power in well defined directions, the radome needs to absorb energy instead and keep the reflections from the hostile radiation low. The rasorber concept supports this desired feature. Rasorbers are thus not PEC backed, and can be constructed by combinations of sheets with metallic as well as lossy periodically arranged patterns imbedded in supporting slabs, see *e.g.*, [18, 24].

The paper is organized such that we in Section 2 and 3 present the geometry of the problem and some prerequisities *e.g.*, the Maxwell equations, constitutive relations and the fundamental equation. The propagators as solutions to the fundamental equation for a general stratified media are introduced in Section 4. In Section 5 we present the generalization of the propagator method, where thin, homogeneous, in general anisotropic, resistive sheets are taken into account by the usage of a well known approximative impedance boundary condition. Furthermore, Section 5 is concluded with an application of the method to the analysis of single layer and multilayer absorbers *i.e.*, Salisbury and Jaumann absorbers. Section 6 continues with the generalization of the propagator method to handle the problem with an arbitrary number of metallic sheets consisting of resistive patch type elements imbedded in supporting linear, bianisotropic slabs. The solution of both the case of finite number of patch elements and the case where the elements are periodically arranged *i.e.*, periodic case is shown by the use of the Galerkin method. Section 7 presents some numerical examples where comparison to data presented in the litterature as well as measured data are shown. An appendix with important results and expressions derived and presented in earlier published work ends this paper.

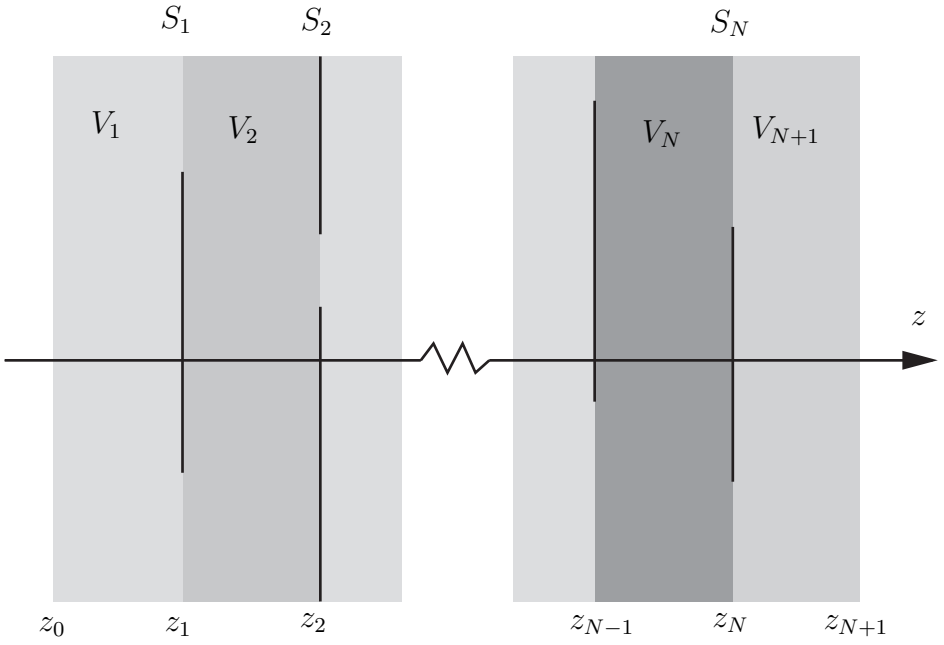

Figure 1: The geometry of the problem with metallic or resistive sheets at $z = z_1, \ldots, z_N$.

2 Geometry

The theory in this paper is formulated for planar structures illustrated by Figure 1. The structure consitutes of N thin sheets of perfectly conducting or resisitive[1], scatterers denoted by $S_1, S_2, \ldots, S_N$ with locations $z = z_n$, $n = 1, 2, \ldots, N$. The sheets $S_1, S_2, \ldots, S_N$ are furthermore supported by bianisotropic slabs occupying the regions $V_1, V_2, \ldots, V_{N+1}$, and the ends of the structure are represented by the coordinates z_0 and z_{N+1}. Notice that the coordinate system is choosen such that the location of the thin scatterers satisfies

$$z_0 < z_1 < z_2 < \cdots < z_{N-1} < z_N < z_{N+1}$$

The space outside the slabs is assumed to be vacuous and the sources of the problem are confined to the regions located to the left and/or the right of the slabs in Figure 1, *i.e.*, the sources are contained in the vacuous half-spaces $z < z_0$ and $z > z_{N+1}$. The dynamics of the fields inside the slabs is modeled by the time-harmonic ($e^{-i\omega t}$) Maxwell equations in a source-free region *i.e.*,

$$\begin{cases} \nabla \times \boldsymbol{E} = ik_0 c_0 \boldsymbol{B} \\ \eta_0 \nabla \times \boldsymbol{H} = -ik_0 c_0 \eta_0 \boldsymbol{D} \end{cases} \tag{2.1}$$

[1]The impedance boundary condition is not restricted to pure resistances. The imposed impedance is in general a complex quantity, which also can be a function of frequency modelling *e.g.*, RCL or LC circuits.

where the permittivity and permeability of vacuum are denoted by ϵ_0 and μ_0, respectively, $c_0 = 1/\sqrt{\epsilon_0\mu_0}$ is the speed of light in vacuum, $\eta_0 = \sqrt{\mu_0/\epsilon_0}$ is the intrinsic impedance of vacuum, and $k_0 = \omega/c_0$ is the vacuum wave number. The magnetic flux vector $\boldsymbol{B}$ and displacement field $\boldsymbol{D}$ on the right-hand side of (2.1) can be expressed in terms of the electric and magnetic field $\boldsymbol{E}$ and $\boldsymbol{H}$, respectively, by the use of the constitutive relations. The time harmonic constitutive relations of a general bianisotropic medium [22] is given by

$$\begin{cases} \boldsymbol{D} = \epsilon_0 \{\boldsymbol{\epsilon} \cdot \boldsymbol{E} + \eta_0 \boldsymbol{\xi} \cdot \boldsymbol{H}\} \\ \boldsymbol{B} = \dfrac{1}{c_0} \{\boldsymbol{\zeta} \cdot \boldsymbol{E} + \eta_0 \boldsymbol{\mu} \cdot \boldsymbol{H}\} \end{cases} \tag{2.2}$$

The bianisotropic medium is the most general linear complex medium comprising at most 36 different scalar constitutive parameters or functions *i.e.*, the bianisotropic slabs are not restricted to be homogeneous, which means that the slabs may be functions of depth z and/or angular frequency ω (dispersive media). In the lateral directions, x- and y-directions, however it is assumed that the material parameters are constant.

The dyadics $\boldsymbol{\epsilon}$ and $\boldsymbol{\mu}$ are the permittivity and permeability dyadics respectively, which for general anisotropic materials comprise nine paremeters each *i.e.*,

$$\begin{cases} \boldsymbol{D} = \epsilon_0 \boldsymbol{\epsilon} \cdot \boldsymbol{E} \\ \boldsymbol{B} = \dfrac{1}{c_0} \eta_0 \boldsymbol{\mu} \cdot \boldsymbol{H} \end{cases} \tag{2.3}$$

For isotropic medium $\boldsymbol{\epsilon}$ and $\boldsymbol{\mu}$ are proportional to the identity dyadic *i.e.*,

$$\begin{cases} \boldsymbol{D} = \epsilon_0 \epsilon \boldsymbol{E} \\ \boldsymbol{B} = \dfrac{1}{c_0} \eta_0 \mu \boldsymbol{H} \end{cases} \tag{2.4}$$

2.1 Decomposition of dyadics

For the pupose of studying wave propagation problems in layered bianisotropic structures by the concept of propagators, [29] is it appropriate to decompose each three-dimensional constitutive dyadic $\mathbf{A}$, according to[2]

$$\mathbf{A} = \mathbf{A}_{\perp\perp} + \hat{\boldsymbol{z}}\boldsymbol{A}_z + \boldsymbol{A}_\perp \hat{\boldsymbol{z}} + \hat{\boldsymbol{z}} A_{zz} \hat{\boldsymbol{z}} \tag{2.5}$$

[2]Generally, all linear transformations $\mathbf{A}$ can be decomposed into components parallel and perpendicular to an arbirary unit vector $\hat{\boldsymbol{n}}$ according to

$$\mathbf{A} = (\mathbf{I}_\perp + \hat{\boldsymbol{n}}\hat{\boldsymbol{n}}) \cdot \mathbf{A} \cdot (\mathbf{I}_\perp + \hat{\boldsymbol{n}}\hat{\boldsymbol{n}}) = \mathbf{A}_{\perp\perp} + \hat{\boldsymbol{n}}\boldsymbol{A}_n + \boldsymbol{A}_\perp \hat{\boldsymbol{n}} + \hat{\boldsymbol{n}} A_{nn} \hat{\boldsymbol{n}}$$

where

$$\mathbf{I}_\perp = \mathbf{I} - \hat{\boldsymbol{n}}\hat{\boldsymbol{n}}$$

is a projection dyadic *i.e.*, a linear transformation that projects an arbitrary vector into a plane with unit normal $\hat{\boldsymbol{n}}$.

where

$$\begin{cases} \mathbf{A}_{\perp\perp} = \mathbf{I}_2 \cdot \mathbf{A} \cdot \mathbf{I}_2 \\ A_{zz} = \hat{\boldsymbol{z}} \cdot \mathbf{A} \cdot \hat{\boldsymbol{z}} \end{cases} \qquad \begin{cases} \boldsymbol{A}_z = \hat{\boldsymbol{z}} \cdot \mathbf{A} \cdot \mathbf{I}_2 \\ \boldsymbol{A}_\perp = \mathbf{I}_2 \cdot \mathbf{A} \cdot \hat{\boldsymbol{z}} \end{cases}$$

The dyadic $\mathbf{A}_{\perp\perp}$ is a two-dimensional dyadic in the x-y plane and the vectors $\boldsymbol{A}_z$ and $\boldsymbol{A}_\perp$ are two two-dimensional vectors in this plane. A_{zz} is a scalar.

Thus, the four dyadics $\boldsymbol{\epsilon}$, $\boldsymbol{\xi}$, $\boldsymbol{\zeta}$ and $\boldsymbol{\mu}$ in the constitutive relations (2.2) for a general bianisotropic medium can be decomposed in tangential and normal parts according to (2.5) *i.e.*,

$$\begin{cases} \boldsymbol{\epsilon} = \boldsymbol{\epsilon}_{\perp\perp} + \hat{\boldsymbol{z}}\boldsymbol{\epsilon}_z + \boldsymbol{\epsilon}_\perp\hat{\boldsymbol{z}} + \hat{\boldsymbol{z}}\epsilon_{zz}\hat{\boldsymbol{z}} \\ \boldsymbol{\xi} = \boldsymbol{\xi}_{\perp\perp} + \hat{\boldsymbol{z}}\boldsymbol{\xi}_z + \boldsymbol{\xi}_\perp\hat{\boldsymbol{z}} + \hat{\boldsymbol{z}}\xi_{zz}\hat{\boldsymbol{z}} \\ \boldsymbol{\zeta} = \boldsymbol{\zeta}_{\perp\perp} + \hat{\boldsymbol{z}}\boldsymbol{\zeta}_z + \boldsymbol{\zeta}_\perp\hat{\boldsymbol{z}} + \hat{\boldsymbol{z}}\zeta_{zz}\hat{\boldsymbol{z}} \\ \boldsymbol{\mu} = \boldsymbol{\mu}_{\perp\perp} + \hat{\boldsymbol{z}}\boldsymbol{\mu}_z + \boldsymbol{\mu}_\perp\hat{\boldsymbol{z}} + \hat{\boldsymbol{z}}\mu_{zz}\hat{\boldsymbol{z}} \end{cases}$$

3 Lateral Fourier transform of the fields

The analysis in this paper is not restricted to plane wave incidence by the fact that the fields can be decomposed into a spectrum of plane waves. Due to the planar geometry presented in Section 2, the plane wave decomposition is acomplished by taking the Fourier transform with respect to the lateral position vector $\boldsymbol{\rho} = \hat{\boldsymbol{x}}x + \hat{\boldsymbol{y}}y$. The Fourier transform is defined by

$$\boldsymbol{E}(\boldsymbol{k}_t, z) = \iint_{-\infty}^{\infty} \boldsymbol{E}(\boldsymbol{r}) e^{-i\boldsymbol{k}_t\cdot\boldsymbol{\rho}}\, dx\, dy$$

where the tangential wave vector $\boldsymbol{k}_t = \hat{\boldsymbol{x}}k_x + \hat{\boldsymbol{y}}k_y$ is real-valued and fixed but arbitrary. The inverse is

$$\boldsymbol{E}(\boldsymbol{r}) = \frac{1}{4\pi^2} \iint_{-\infty}^{\infty} \boldsymbol{E}(\boldsymbol{k}_t, z) e^{i\boldsymbol{k}_t\cdot\boldsymbol{\rho}}\, dk_x\, dk_y$$

In this paper the argument of the field indicates whether the field itself $\boldsymbol{E}(\boldsymbol{r})$ or its Fourier transform $\boldsymbol{E}(\boldsymbol{k}_t, z)$ with respect to $\boldsymbol{\rho}$ is intended.

The lateral wave number $k_t = \sqrt{k_x^2 + k_y^2}$ is a non-negative real number, which in general is non-zero, and then it is appropriate to make use of the orthogonal basis defined by

$$\begin{cases} \hat{\boldsymbol{e}}_\parallel(\boldsymbol{k}_t) = \boldsymbol{k}_t/k_t \\ \hat{\boldsymbol{e}}_\perp(\boldsymbol{k}_t) = \hat{\boldsymbol{z}} \times \hat{\boldsymbol{e}}_\parallel(\boldsymbol{k}_t) \end{cases}$$

for the representation of lateral vectors in the x-y-plane [29].

3.1 The Fundamental equation

The time-harmonic fields can be uniquely decomposed into their lateral components, $\boldsymbol{E}_{xy}(\boldsymbol{k}_t, z)$ and $\eta_0 \boldsymbol{H}_{xy}(\boldsymbol{k}_t, z)$, and longitudinal ($z$) components, $E_z(\boldsymbol{k}_t, z)$ and $\eta_0 H_z(\boldsymbol{k}_t, z)$ according to

$$\begin{cases} \boldsymbol{E}(\boldsymbol{k}_t, z) = \boldsymbol{E}_{xy}(\boldsymbol{k}_t, z) + \hat{\boldsymbol{z}} E_z(\boldsymbol{k}_t, z) \\ \boldsymbol{H}(\boldsymbol{k}_t, z) = \boldsymbol{H}_{xy}(\boldsymbol{k}_t, z) + \hat{\boldsymbol{z}} H_z(\boldsymbol{k}_t, z) \end{cases}$$

By making use of these decompositions in the Maxwell equations (2.1), it follows that the longitudinal field components can be eliminated and that the Maxwell equations for a bianisotropic medium can be transformed into a system of coupled ordinary differential equations (ODE) *i.e.*, the fundamental equation for one-dimensional time-harmonic wave propagation [29]

$$\frac{\mathrm{d}}{\mathrm{d}z} \begin{pmatrix} \boldsymbol{E}_{xy}(\boldsymbol{k}_t, z) \\ \hat{\boldsymbol{z}} \times \eta_0 \boldsymbol{H}_{xy}(\boldsymbol{k}_t, z) \end{pmatrix} = ik_0 \mathbf{M}(\boldsymbol{k}_t, z) \cdot \begin{pmatrix} \boldsymbol{E}_{xy}(\boldsymbol{k}_t, z) \\ \hat{\boldsymbol{z}} \times \eta_0 \boldsymbol{H}_{xy}(\boldsymbol{k}_t, z) \end{pmatrix} \tag{3.1}$$

where $\mathbf{M}(\boldsymbol{k}_t, z)$ is a 4×4 complex-valued dyadic. In a bianisotropic media modelled by the constitutive relations (2.2) the map $\mathbf{M}(\boldsymbol{k}_t, z)$ is explicitly given by [29]

$$\mathbf{M}(\boldsymbol{k}_t, z) = \begin{pmatrix} -\mathbf{J} \cdot \boldsymbol{\zeta}_{\perp\perp} & \mathbf{J} \cdot \boldsymbol{\mu}_{\perp\perp} \cdot \mathbf{J} \\ -\boldsymbol{\epsilon}_{\perp\perp} & \boldsymbol{\xi}_{\perp\perp} \cdot \mathbf{J} \end{pmatrix} + \begin{pmatrix} \boldsymbol{k}_t/k_0 - \mathbf{J} \cdot \boldsymbol{\zeta}_{\perp} & -\mathbf{J} \cdot \boldsymbol{\mu}_{\perp} \\ -\boldsymbol{\epsilon}_{\perp} & \mathbf{J} \cdot \boldsymbol{k}_t/k_0 - \boldsymbol{\xi}_{\perp} \end{pmatrix}$$
$$+ \frac{1}{\epsilon_{zz}\mu_{zz} - \xi_{zz}\zeta_{zz}} \begin{pmatrix} -\mu_{zz}\boldsymbol{\epsilon}_z - \xi_{zz}\mathbf{J} \cdot \boldsymbol{k}_t/k_0 + \xi_{zz}\boldsymbol{\zeta}_z & \mu_{zz}\boldsymbol{k}_t/k_0 + \mu_{zz}\boldsymbol{\xi}_z \cdot \mathbf{J} - \xi_{zz}\boldsymbol{\mu}_z \cdot \mathbf{J} \\ \zeta_{zz}\boldsymbol{\epsilon}_z + \epsilon_{zz}\mathbf{J} \cdot \boldsymbol{k}_t/k_0 - \epsilon_{zz}\boldsymbol{\zeta}_z & -\zeta_{zz}\boldsymbol{k}_t/k_0 - \zeta_{zz}\boldsymbol{\xi}_z \cdot \mathbf{J} + \epsilon_{zz}\boldsymbol{\mu}_z \cdot \mathbf{J} \end{pmatrix}$$

where the material dyadic decomposition according to Section 2.1 has been used and $\mathbf{J} = \hat{\boldsymbol{z}} \times \mathbf{I}_2$ represents a rotation of $\pi/2$ around the z-axis, and $\mathbf{I}_2 = \hat{\boldsymbol{e}}_{\parallel}\hat{\boldsymbol{e}}_{\parallel} + \hat{\boldsymbol{e}}_{\perp}\hat{\boldsymbol{e}}_{\perp}$ is the identity dyadic in $\mathbb{R}^2$ for lateral vectors. Notice that the four dyadics $\boldsymbol{\epsilon}$, $\boldsymbol{\xi}$, $\boldsymbol{\zeta}$ and $\boldsymbol{\mu}$ depend on z for materials that are stratified in the z direction. In homogeneous regions, the map $\mathbf{M}(\boldsymbol{k}_t, z)$ is independent of z, and, specifically, in a vacuous region $\mathbf{M}(\boldsymbol{k}_t)$ is

$$\mathbf{M}_0(\boldsymbol{k}_t) = \begin{pmatrix} \mathbf{0} & -\mathbf{I}_2 + \frac{1}{k_0^2}\boldsymbol{k}_t\boldsymbol{k}_t \\ -\mathbf{I}_2 - \frac{1}{k_0^2}\boldsymbol{k}_t \times (\boldsymbol{k}_t \times \mathbf{I}_2) & \mathbf{0} \end{pmatrix} \tag{3.2}$$

4 Wave propagation by the notion of propagators

A formal solution of the fundamental equation (3.1) can be written [29]

$$\begin{pmatrix} \boldsymbol{E}_{xy}(\boldsymbol{k}_t, z) \\ \eta_0 \mathbf{J} \cdot \boldsymbol{H}_{xy}(\boldsymbol{k}_t, z) \end{pmatrix} = \mathbf{P}(\boldsymbol{k}_t, z, z_1) \cdot \begin{pmatrix} \boldsymbol{E}_{xy}(\boldsymbol{k}_t, z_1) \\ \eta_0 \mathbf{J} \cdot \boldsymbol{H}_{xy}(\boldsymbol{k}_t, z_1) \end{pmatrix}$$

where the propagator $\mathbf{P}$ is a linear map (4×4 complex-valued dyadic) mapping the tangential electric and magnetic fields from z_1 to z. For a homogeneous material, an explicit solution of (3.1) can be found, and in this case the propagator is[3]

$$\mathbf{P}(\boldsymbol{k}_t, z, z_1) = e^{ik_0(z-z_1)\mathbf{M}(\boldsymbol{k}_t)} \tag{4.1}$$

[3]The order of the z-arguments in the propagator is important.

A general result for the propagator of a single homogeneous layer can be obtained using the Cayley-Hamilton theorem, see Appendix A, provided the eigenvalues of the fundamental dyadic, $\mathbf{M}$, are distinct [29]. Since the exponential is an entire function, the Cayley-Hamilton theorem gives ($d = z - z_1$)

$$e^{ik_0 d\mathbf{M}} = q_0(k_0 d)\mathbf{I}_4 + q_2(k_0 d)\mathbf{M}\cdot\mathbf{M} + (q_1(k_0 d)\mathbf{I}_4 + q_3(k_0 d)\mathbf{M}\cdot\mathbf{M})\cdot\mathbf{M}$$

where the coefficients, $q_l(k_0 d)$, $l = 1, 2, 3, 4$, are given by the system of linear equations

$$e^{ik_0 d\lambda_l} = q_0(k_0 d) + q_2(k_0 d)\lambda_l^2 + \left(q_1(k_0 d) + q_3(k_0 d)\lambda_l^2\right)\lambda_l, \qquad l = 1, 2, 3, 4 \tag{4.2}$$

provided the eigenvalues, λ_l, $l = 1, 2, 3, 4$, of the fundamental dyadic, $\mathbf{M}$, are distinct. This can generally be assumed unless the medium is isotropic or Tellegen [29]. Let

$$V = \begin{pmatrix} 1 & \lambda_1 & \lambda_1^2 & \lambda_1^3 \\ 1 & \lambda_2 & \lambda_2^2 & \lambda_2^3 \\ 1 & \lambda_3 & \lambda_3^2 & \lambda_3^3 \\ 1 & \lambda_4 & \lambda_4^2 & \lambda_4^3 \end{pmatrix}$$

The system of linear equations (4.2) and its solution can then formally be written

$$e = V\cdot q, \qquad q = V^{-1}\cdot e$$

where

$$e = \begin{pmatrix} e^{ik_0 d\lambda_1} \\ e^{ik_0 d\lambda_2} \\ e^{ik_0 d\lambda_3} \\ e^{ik_0 d\lambda_4} \end{pmatrix}, \qquad q = \begin{pmatrix} q_0(k_0 d) \\ q_1(k_0 d) \\ q_2(k_0 d) \\ q_3(k_0 d) \end{pmatrix}$$

For a homogeneous isotropic slab ($\xi = \zeta = \mathbf{0}$, $\epsilon = \epsilon\mathbf{I}_3$, $\mu = \mu\mathbf{I}_3$), the fundamental dyadic is explicitly given by

$$\mathbf{M}(\boldsymbol{k}_t) = \begin{pmatrix} \mathbf{0} & -\mu\mathbf{I}_2 + \frac{1}{\epsilon k_0^2}\boldsymbol{k}_t\boldsymbol{k}_t \\ -\epsilon\mathbf{I}_2 - \frac{1}{\mu k_0^2}\mathbf{J}\cdot\boldsymbol{k}_t\boldsymbol{k}_t\cdot\mathbf{J} & \mathbf{0} \end{pmatrix}$$

with eigenvalues [29]

$$\lambda^2 = \epsilon\mu - k_t^2/k_0^2 \tag{4.3}$$

The single-slab propagator (4.1) can then be shown being given by ($d = z - z_1$), [29]

$$\mathbf{P}(\boldsymbol{k}_t, z, z_1) = e^{ik_0 d\mathbf{M}(\boldsymbol{k}_t)} = \mathbf{I}_4\cos(k_0 d\lambda) + \frac{i}{\lambda}\mathbf{M}(\boldsymbol{k}_t)\sin(k_0 d\lambda) \tag{4.4}$$

From (4.3) it is furthermore seen that

$$k_0^2\lambda^2 = k_0^2\epsilon\mu - k_t^2 = k^2 - k_t^2$$

and thus the longitudinal wave number k_z is given by (k assumed real)

$$k_z = \left(k^2 - k_t^2\right)^{1/2} = \begin{cases} \sqrt{k^2 - k_t^2} \text{ for } k_t < k \\ i\sqrt{k_t^2 - k^2} \text{ for } k_t > k \end{cases}$$

Thus, the propagator for a homogeneous isotropic slab (4.4) can be rewritten in the final form

$$\mathbf{P}(\boldsymbol{k}_t, z, z_1) = \mathbf{I}_4 \cos(k_z d) + \frac{ik_0}{k_z}\mathbf{M}(\boldsymbol{k}_t)\sin(k_z d) \tag{4.5}$$

See, [29] for further details and other explicit expressions of propagators.

4.1 Propagators in stratified media

Consider the stratified structure shown in Figure 1, and assume that there are no metallic or resistive sheets at $z = z_1, \ldots, z_N$ *i.e.*, the structure is assumed to be a layered dielectric structure. Let $\mathbf{M}_j(\boldsymbol{k}_t)$, $j = 1, \ldots, N+1$, be the dyadics modelling the materials of the corresponding regions $V_1, V_2, \ldots, V_{N+1}$ illustrated in Figure 1. All slabs are furthermore assumed homogeneous and the ends of the structure are represented by the coordinates z_0 and z_{N+1}, and the space outside the slabs is vacuous. Thus, $\mathbf{M}_{N+2}(\boldsymbol{k}_t) = \mathbf{M}_0(\boldsymbol{k}_t)$, where $\mathbf{M}_0(\boldsymbol{k}_t)$ is explicitly given by (3.2), *i.e.*, $\epsilon = \mu = \mathbf{I}_3$ and $\xi = \zeta = \mathbf{0}$ in these half spaces. Since the tangential electric and magnetic fields are continuous at the boundaries repeated use of the propagator (4.1) gives [29]

$$\begin{pmatrix} \boldsymbol{E}_{xy}(\boldsymbol{k}_t, z_{N+1}) \\ \eta_0 \mathbf{J} \cdot \boldsymbol{H}_{xy}(\boldsymbol{k}_t, z_{N+1}) \end{pmatrix} = \mathbf{P}(\boldsymbol{k}_t, z_{N+1}, z_0) \cdot \begin{pmatrix} \boldsymbol{E}_{xy}(\boldsymbol{k}_t, z_0) \\ \eta_0 \mathbf{J} \cdot \boldsymbol{H}_{xy}(\boldsymbol{k}_t, z_0) \end{pmatrix}$$

where the propagator for the whole stratified structure is

$$\mathbf{P}(\boldsymbol{k}_t, z_{N+1}, z_0) = e^{ik_0(z_{N+1}-z_N)\mathbf{M}_{N+1}(\boldsymbol{k}_t)} \cdot \ldots \cdot e^{ik_0(z_2-z_1)\mathbf{M}_2(\boldsymbol{k}_t)} \cdot e^{ik_0(z_1-z_0)\mathbf{M}_1(\boldsymbol{k}_t)}$$

The corresponding relations for the two vacuous half spaces are [21]

$$\begin{pmatrix} \boldsymbol{E}_{xy}(\boldsymbol{k}_t, z) \\ \eta_0 \mathbf{J} \cdot \boldsymbol{H}_{xy}(\boldsymbol{k}_t, z) \end{pmatrix} = \mathbf{P}(\boldsymbol{k}_t, z, z_0) \cdot \begin{pmatrix} \boldsymbol{E}_{xy}(\boldsymbol{k}_t, z_0) \\ \eta_0 \mathbf{J} \cdot \boldsymbol{H}_{xy}(\boldsymbol{k}_t, z_0) \end{pmatrix}, \qquad z < z_0 \tag{4.6}$$

$$\begin{pmatrix} \boldsymbol{E}_{xy}(\boldsymbol{k}_t, z) \\ \eta_0 \mathbf{J} \cdot \boldsymbol{H}_{xy}(\boldsymbol{k}_t, z) \end{pmatrix} = \mathbf{P}(\boldsymbol{k}_t, z, z_{N+1}) \cdot \begin{pmatrix} \boldsymbol{E}_{xy}(\boldsymbol{k}_t, z_{N+1}) \\ \eta_0 \mathbf{J} \cdot \boldsymbol{H}_{xy}(\boldsymbol{k}_t, z_{N+1}) \end{pmatrix}, \qquad z > z_{N+1} \tag{4.7}$$

where the propagators in (4.6) and (4.7) having the form (4.5) with the fundamental dyadic $\mathbf{M}(\boldsymbol{k}_t) = \mathbf{M}_0(\boldsymbol{k}_t)$ explicitly given by (3.2).

5 Propagators and homogeneous resistive sheets

The theory of the propagator method presented in [29] cannot accommodate thin resistive sheets. This section presents a generalization of the method where thin homogeneous resistive sheets are taken into account by the use of a well known approximative impedance boundary condition [31]. It is shown that the impedance boundary condition can be introduced into the concept of propagators and the theory is formulated for planar structures of one or several homogeneous resistive sheets imbedded in the supporting slabs.

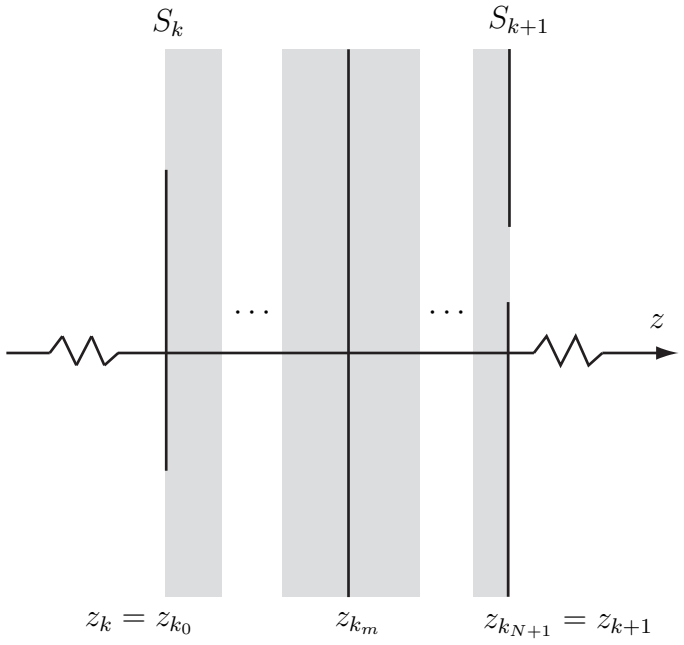

Figure 2: The geometry of a subsection of the structure shown in Figure 1 with one resistive sheet at $z = z_{k_m}$ inside a stratified structure with N layers between the boundaries at $z = z_k$ and $z = z_{k+1}$.

Any number of resistive sheets can be introduced in the structure shown in Figure 1. Assume that one homogeneous resistive sheet islocated between the boundaries of $z = z_k$ and $z = z_{k+1}$, see Figure 2. Furthermore, assume that the substructure between $z = z_k$ and $z = z_{k+1}$ is stratified and consists of $N + 1$ bianisotropic layers. As was pointed out in the preceeding section, the concept of propagators relates the total transverse fields to each other, and for a general bianisotropic stratified structure without any resistive sheet, the transverse fields are continuous at each location z_{k_n} where $n = 1, 2, \ldots, N$ *i.e.*,

$$\begin{cases} \boldsymbol{E}_{xy}(\boldsymbol{k}_t, z_{k_n}^-) = \boldsymbol{E}_{xy}(\boldsymbol{k}_t, z_{k_n}^+) \\ \eta_0 \mathbf{J} \cdot \boldsymbol{H}_{xy}(\boldsymbol{k}_t, z_{k_n}^-) = \eta_0 \mathbf{J} \cdot \boldsymbol{H}_{xy}(\boldsymbol{k}_t, z_{k_n}^+) \end{cases} \tag{5.1}$$

Introducing the resistive sheet with surface resistivity Z_{k_m}, which in general is complex-valued, at z_{k_m}, we make use of the following impedance boundary condition at z_{k_m}

$$\begin{cases} \boldsymbol{E}_{xy}(\boldsymbol{k}_t, z_{k_m}^+) = \boldsymbol{E}_{xy}(\boldsymbol{k}_t, z_{k_m}^-) \\ \eta_0 \mathbf{J} \cdot \big(\boldsymbol{H}_{xy}(\boldsymbol{k}_t, z_{k_m}^+) - \boldsymbol{H}_{xy}(\boldsymbol{k}_t, z_{k_m}^-) \big) = \eta_0 Z_{k_m}^{-1} \boldsymbol{E}_{xy}(\boldsymbol{k}_t, z_{k_m}^-) \end{cases} \tag{5.2}$$

The boundary condition (5.2) is well known and used as an approximate boundary condition for thin structures, see [12, 15, 31]. Letting $Z_{k_m} \to \infty$, it is seen that the boundary conditions for pure dielectric interfaces (5.1) is obtained, and in the limit $Z_{k_m} \to 0$ the location z_{k_m} corresponds to a PEC boundary where the magnetic field

$\boldsymbol{H}_{xy}(\boldsymbol{k}_t, z_{k_m})$ has a jump discontinuity *i.e.*, $Z_{k_m}^{-1}\boldsymbol{E}_{xy}(\boldsymbol{k}_t, z_{k_m}^-) \to \boldsymbol{J}_S(\boldsymbol{k}_t, z_{k_m})$ when $Z_{k_m} \to 0$. See, furthermore Appendix B, about the different type of boundary conditions, considered within the theory of this paper.

The continuity of the tangential electric field implies that we can reformulate (5.2) as

$$\begin{cases} \boldsymbol{E}_{xy}(\boldsymbol{k}_t, z_{k_m}^-) = \boldsymbol{E}_{xy}(\boldsymbol{k}_t, z_{k_m}^+) \\ \eta_0 \mathbf{J} \cdot \big(\boldsymbol{H}_{xy}(\boldsymbol{k}_t, z_{k_m}^-) - \boldsymbol{H}_{xy}(\boldsymbol{k}_t, z_{k_m}^+)\big) = -\eta_0 Z_{k_m}^{-1}\boldsymbol{E}_{xy}(\boldsymbol{k}_t, z_{k_m}^+) \end{cases} \tag{5.3}$$

The propagator formalism is written in dyadic form, and to this end, the boundary condition (5.2) and its equivalent form (5.3) are written in dyadic form

$$\mathbf{Z}^{\pm}(Z) = \begin{pmatrix} \mathbf{Z}_{ee}^{\pm}(Z) & \mathbf{Z}_{em}^{\pm}(Z) \\ \mathbf{Z}_{me}^{\pm}(Z) & \mathbf{Z}_{mm}^{\pm}(Z) \end{pmatrix} = \begin{pmatrix} \mathbf{I}_2 & \mathbf{0} \\ \pm\eta_0 Z^{-1}\mathbf{I}_2 & \mathbf{I}_2 \end{pmatrix} \tag{5.4}$$

The impedance dyadic (5.4) modells an isotropic thin sheet, but can easily be generalized to anisotropic sheets *e.g.*, modelling of parallel wires imbedded in a dielectric [31]. The generalized impedance dyadic for an anisotropic sheet at z_{k_m} is written

$$\mathbf{Z}^{\pm} = \begin{pmatrix} \mathbf{Z}_{ee}^{\pm} & \mathbf{Z}_{em}^{\pm} \\ \mathbf{Z}_{me}^{\pm} & \mathbf{Z}_{mm}^{\pm} \end{pmatrix} = \begin{pmatrix} \mathbf{I}_2 & \mathbf{0} \\ \pm\eta_0 \mathbf{Z}_2^{-1} & \mathbf{I}_2 \end{pmatrix} \tag{5.5}$$

where the dyadic $\mathbf{Z}_2^{-1}$ is a linear map $\mathbb{C}^2 \to \mathbb{C}^2$. The dyadic $\mathbf{Z}^+$ maps the tangential fields through the resistive sheet from the left to the right *i.e.*, from $z_{k_m}^-$ to $z_{k_m}^+$ or in the reverse direction by $\mathbf{Z}^-$. Thus,

$$\begin{pmatrix} \boldsymbol{E}_{xy}(\boldsymbol{k}_t, z_{k_{m+1}}^-) \\ \eta_0 \mathbf{J} \cdot \boldsymbol{H}_{xy}(\boldsymbol{k}_t, z_{k_{m+1}}^-) \end{pmatrix} = \mathbf{P}(\boldsymbol{k}_t, z_{k_{m+1}}, z_{k_m}) \cdot \mathbf{Z}^+ \cdot \begin{pmatrix} \boldsymbol{E}_{xy}(\boldsymbol{k}_t, z_{k_m}^-) \\ \eta_0 \mathbf{J} \cdot \boldsymbol{H}_{xy}(\boldsymbol{k}_t, z_{k_m}^-) \end{pmatrix}$$

or

$$\begin{pmatrix} \boldsymbol{E}_{xy}(\boldsymbol{k}_t, z_{k_{m-1}}^+) \\ \eta_0 \mathbf{J} \cdot \boldsymbol{H}_{xy}(\boldsymbol{k}_t, z_{k_{m-1}}^+) \end{pmatrix} = \mathbf{P}(\boldsymbol{k}_t, z_{k_{m-1}}, z_{k_m}) \cdot \mathbf{Z}^- \cdot \begin{pmatrix} \boldsymbol{E}_{xy}(\boldsymbol{k}_t, z_{k_m}^+) \\ \eta_0 \mathbf{J} \cdot \boldsymbol{H}_{xy}(\boldsymbol{k}_t, z_{k_m}^+) \end{pmatrix}$$

where the propagator $\mathbf{P}$ for a general linear homogeneous medium is given by (4.1).

Similarly, if there is a resistive sheet at z_0 in Figure 1, modelled with the impedance dyadic $\mathbf{Z}_0^{\pm}$, for the vacuous half space to the left, we have

$$\begin{pmatrix} \boldsymbol{E}_{xy}(\boldsymbol{k}_t, z) \\ \eta_0 \mathbf{J} \cdot \boldsymbol{H}_{xy}(\boldsymbol{k}_t, z) \end{pmatrix} = \mathbf{P}(\boldsymbol{k}_t, z, z_0) \cdot \mathbf{Z}_0^- \cdot \begin{pmatrix} \boldsymbol{E}_{xy}(\boldsymbol{k}_t, z_0^+) \\ \eta_0 \mathbf{J} \cdot \boldsymbol{H}_{xy}(\boldsymbol{k}_t, z_0^+) \end{pmatrix}, \qquad z < z_0$$

or in case of a resistive sheet at z_{N+1} with impedance dyadic $\mathbf{Z}_{N+1}^{\pm}$, we have for the vacuous half space to the right

$$\begin{pmatrix} \boldsymbol{E}_{xy}(\boldsymbol{k}_t, z) \\ \eta_0 \mathbf{J} \cdot \boldsymbol{H}_{xy}(\boldsymbol{k}_t, z) \end{pmatrix} = \mathbf{P}(\boldsymbol{k}_t, z, z_{N+1}) \cdot \mathbf{Z}_{N+1}^+ \cdot \begin{pmatrix} \boldsymbol{E}_{xy}(\boldsymbol{k}_t, z_{N+1}^-) \\ \eta_0 \mathbf{J} \cdot \boldsymbol{H}_{xy}(\boldsymbol{k}_t, z_{N+1}^-) \end{pmatrix}, \qquad z > z_{N+1}$$

The propagators $\mathbf{P}(\boldsymbol{k}_t, z, z_0)$ and $\mathbf{P}(\boldsymbol{k}_t, z, z_{N+1})$, respectively, have the form (4.5) with the fundamental dyadic $\mathbf{M}(\boldsymbol{k}_t) = \mathbf{M}_0(\boldsymbol{k}_t)$ explicitly given by (3.2).

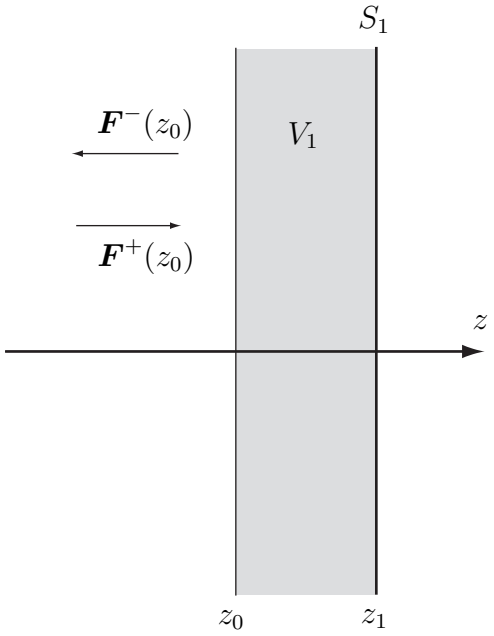

Figure 3: The geometry of a Salisbury screen *i.e.*, a structure with one resistive sheet at $z = z_0$ backed with a PEC located at $z = z_1$.

5.1 The Salisbury screen

The basic geometry of a Salisbury screen is shown in Figure 3. Consider first the reflection dyadic for the PEC backed structure with the resistive sheet absent *i.e.*, [29]

$$\mathbf{r}(\boldsymbol{k}_t, z_1, z_0) = -\left(\mathbf{P}_{ee} + \mathbf{P}_{em} \cdot \mathbf{W}^{-1}\right)^{-1} \cdot \left(\mathbf{P}_{ee} - \mathbf{P}_{em} \cdot \mathbf{W}^{-1}\right)(\boldsymbol{k}_t, z_1, z_0) \tag{5.6}$$

where the block dyadics $\mathbf{P}_{ee}$ and $\mathbf{P}_{em}$ are defined by the propagator decomposition

$$\mathbf{P}(\boldsymbol{k}_t, z_{n+1}, z_n) = \begin{pmatrix} \mathbf{P}_{ee}(\boldsymbol{k}_t, z_{n+1}, z_n) & \mathbf{P}_{em}(\boldsymbol{k}_t, z_{n+1}, z_n) \\ \mathbf{P}_{me}(\boldsymbol{k}_t, z_{n+1}, z_n) & \mathbf{P}_{mm}(\boldsymbol{k}_t, z_{n+1}, z_n) \end{pmatrix}$$

and the wave splitting dyadic $\mathbf{W}^{-1}$ is given by

$$\mathbf{W}^{-1}(\boldsymbol{k}_t) = \frac{k_0}{k_z}\left(\mathbf{I}_2 + \frac{1}{k_0^2}\boldsymbol{k}_t \times (\boldsymbol{k}_t \times \mathbf{I}_2)\right) = \hat{\boldsymbol{e}}_{\parallel}\hat{\boldsymbol{e}}_{\parallel}\frac{k_0}{k_z} + \hat{\boldsymbol{e}}_{\perp}\hat{\boldsymbol{e}}_{\perp}\frac{k_z}{k_0}$$

By introducing a resistive sheet at z_0 with surface resistivity Z_0 (isotropic case) we can express the boundary condition at z_1 (PEC) according to

$$\begin{aligned}\begin{pmatrix} \mathbf{0} \\ -\eta_0 \boldsymbol{J}_S \end{pmatrix} &= \begin{pmatrix} \boldsymbol{E}_{xy}(\boldsymbol{k}_t, z_1) \\ \eta_0 \mathbf{J} \cdot \boldsymbol{H}_{xy}(\boldsymbol{k}_t, z_1) \end{pmatrix} \\ &= \mathbf{P}(\boldsymbol{k}_t, z_1, z_0) \cdot \mathbf{Z}^+(Z_0) \cdot \begin{pmatrix} \mathbf{I}_2 & \mathbf{I}_2 \\ -\mathbf{W}^{-1} & \mathbf{W}^{-1} \end{pmatrix} \cdot \begin{pmatrix} \boldsymbol{F}^+(z_0) \\ \mathbf{r} \cdot \boldsymbol{F}^+(z_0) \end{pmatrix}\end{aligned}$$

where $\boldsymbol{F}^+(z_0)$ denotes the excitation of the structure[4] at z_0 and $\mathbf{Z}^+(Z_0)$ is given by (5.4). The upper equation of the boundary condition gives the reflection dyadic in case of a resistive sheet at z_0. The result is

$$\begin{aligned}\mathbf{r}(\boldsymbol{k}_t, z_1, z_0) = &- \left(\mathbf{P}_{ee} + \mathbf{P}_{em} \cdot \left(\mathbf{Z}^+_{me}(Z_0) + \mathbf{W}^{-1}\right)\right)^{-1} \\ &\cdot \left(\mathbf{P}_{ee} + \mathbf{P}_{em} \cdot \left(\mathbf{Z}^+_{me}(Z_0) - \mathbf{W}^{-1}\right)\right)(\boldsymbol{k}_t, z_1, z_0)\end{aligned} \tag{5.7}$$

where

$$\mathbf{Z}^+_{me}(Z_0) = \frac{\eta_0}{Z_0}\mathbf{I}_2, \qquad Z_0 \neq 0$$

Letting $Z_0 \to \infty$ in (5.7) it is seen that the result converges to (5.6) *i.e.*, the case without a resistive sheet at z_0. Furthermore, if $Z_0 \to 0$ we obtain the case with a PEC at z_0 and $\mathbf{r}(\boldsymbol{k}_t, z_1, z_0) = -\mathbf{I}_4$ in that case. In the anisotropic case, we simply replace $\mathbf{Z}^+_{me}(Z_0)$ in (5.7) with $\eta_0\mathbf{Z}_2^{-1}(Z_0)$ according to (5.5).

Let the incident electric field at $z = z_0$ be defined by [29]

$$\boldsymbol{E}^i(z_0) = E_0(z_0)\left(\hat{\boldsymbol{e}}_\perp \cos\chi + \hat{\boldsymbol{e}}_\perp \times \hat{\boldsymbol{k}}^+ \sin\chi\right)$$

where $\boldsymbol{k}^+ = \boldsymbol{k}_t + \hat{\boldsymbol{z}}k_z$, χ is the polarization angle, $\chi = 0$ (TE polarization) and $\chi = \pi/2$ (TM polarization) and $E_0(z_0)$ is a complex number determined by the amplitude and phase of the incident field at the front end of the structure. The reflectance R of the structure is then given by [29]

$$R = \left|r_{\parallel\parallel}\sin\chi + r_{\parallel\perp}\cos\chi/\cos\theta_i\right|^2 + \left|r_{\perp\parallel}\cos\theta_i\sin\chi + r_{\perp\perp}\cos\chi\right|^2 \tag{5.8}$$

where θ_i is the angle of incidence defined by $\hat{\boldsymbol{z}} \cdot \hat{\boldsymbol{k}}^+ = \cos\theta_i$ and $r_{\parallel\parallel}$, $r_{\parallel\perp}$, $r_{\perp\parallel}$ and $r_{\perp\perp}$ are the components of the reflection dyadic (5.7) *i.e.*,

$$\mathbf{r}(\boldsymbol{k}_t, z_1, z_0) = \hat{\boldsymbol{e}}_\parallel\hat{\boldsymbol{e}}_\parallel r_{\parallel\parallel} + \hat{\boldsymbol{e}}_\parallel\hat{\boldsymbol{e}}_\perp r_{\parallel\perp} + \hat{\boldsymbol{e}}_\perp\hat{\boldsymbol{e}}_\parallel r_{\perp\parallel} + \hat{\boldsymbol{e}}_\perp\hat{\boldsymbol{e}}_\perp r_{\perp\perp}$$

5.2 Multilayer resistive sheet

The results from Section 5.1 can be generalized to the case of a PEC backed structure with more than one resistive sheet as depicted in Figure 4. The boundary conditions at z_N in this case are

$$\begin{pmatrix}\mathbf{0}\\ -\eta_0\boldsymbol{J}_S\end{pmatrix} = \begin{pmatrix}\boldsymbol{E}_{xy}(\boldsymbol{k}_t, z_N)\\ \eta_0\mathbf{J}\cdot\boldsymbol{H}_{xy}(\boldsymbol{k}_t, z_N)\end{pmatrix} = \mathbf{P}_Z(\boldsymbol{k}_t, z_N, z_0)\cdot\begin{pmatrix}\mathbf{I}_2 & \mathbf{I}_2\\ -\mathbf{W}^{-1} & \mathbf{W}^{-1}\end{pmatrix}\cdot\begin{pmatrix}\boldsymbol{F}^+(z_0)\\ \mathbf{r}\cdot\boldsymbol{F}^+(z_0)\end{pmatrix}$$

where

$$\mathbf{P}_Z(\boldsymbol{k}_t, z_N, z_0) = \left(\prod_{n=1}^{N-1}\mathbf{P}_{n+1}(\boldsymbol{k}_t, z_{n+1}, z_n)\cdot\mathbf{Z}^+_n\right)\cdot\mathbf{P}_1(\boldsymbol{k}_t, z_1, z_0) \tag{5.9}$$

with $\mathbf{Z}^+_n$ in general given by (5.5) and in the isotropic case by (5.4). The upper equation of the boundary condition gives the reflection dyadic and the result is *cf.*, (5.6)

$$\mathbf{r}(\boldsymbol{k}_t, z_N, z_0) = -\left(\mathbf{P}_{Zee} + \mathbf{P}_{Zem}\cdot\mathbf{W}^{-1}\right)^{-1}\cdot\left(\mathbf{P}_{Zee} - \mathbf{P}_{Zem}\cdot\mathbf{W}^{-1}\right)(\boldsymbol{k}_t, z_N, z_0) \tag{5.10}$$

[4]The reflected part of the excitation at z_0 is by definition $\mathbf{r}\cdot\boldsymbol{F}^+(z_0) = \boldsymbol{F}^-(z_0)$.

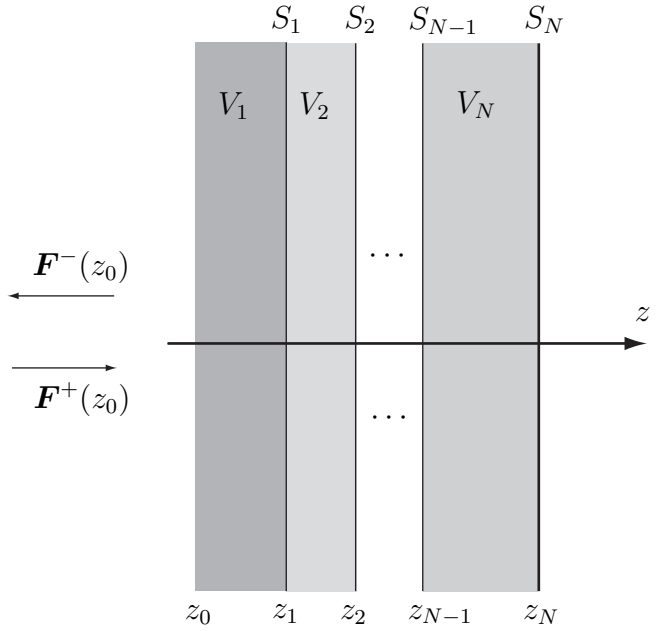

Figure 4: The geometry of a multilayer resistive sheet (Jaumann absorber) *i.e.*, a structure with two or more resistive sheets located at $z_1, z_2, \ldots, z_{N-1}$, backed with a PEC at the boundary $z = z_N$.

where $\mathbf{P}_{Zee}$ and $\mathbf{P}_{Zem}$ denotes the block dyadics of (5.9) written in the form

$$\mathbf{P}_Z(\boldsymbol{k}_t, z_N, z_0) = \begin{pmatrix} \mathbf{P}_{Zee}(\boldsymbol{k}_t, z_N, z_0) & \mathbf{P}_{Zem}(\boldsymbol{k}_t, z_N, z_0) \\ \mathbf{P}_{Zme}(\boldsymbol{k}_t, z_N, z_0) & \mathbf{P}_{Zmm}(\boldsymbol{k}_t, z_N, z_0) \end{pmatrix}$$

Similarily letting $Z_n \to \infty$ for $n = 1, 2, \ldots, N-1$ it is seen that $\mathbf{Z}^+(Z_n) \to \mathbf{I}_4$ ($\mathbf{Z}_n^+ \to \mathbf{I}_4$) for $n = 1, 2, \ldots, N-1$ which implies that (5.10) converges to the case of a PEC backed structure without any resistive sheets *cf.*, (5.6). Furthermore, if letting $Z_n \to 0$ for $n = 1, 2, \ldots, N-1$, we obtain $\mathbf{r}(\boldsymbol{k}_t, z_N, z_0) = -\mathbf{I}_4$. The reflectance R of this structure is computed according to (5.8).

6 Propagators and resistive elements

The theory presented in [21] provides a method for solving scattering problems in planar geometries with an arbitrary number of metallic sheets consisting of aperture or patch type elements imbedded in supporting linear bianisotropic slabs. In this section, we extend the theory in [21] by considering lossy as well as perfect conducting patch type elements by employing the impedance boundary condition discussed in Appendix B.

A summary of the explicit relations between the current distributions and the tangential fields at the screens derived in [21] based on the propagator formalism is presented in Appendix C. In this section, we show how the results from Appendix C

can be used to solve the patch case, where losses are taken into account. It is furthermore shown that results for the metallic case reported in [21] is a special case of the resistive case in the limit when the conductivity goes to infinity. In Section 6.1 we consider the case with a finite number of elements and employ the Galerkin method, and in Section 6.2 we adress the case where the elements are periodically arranged *i.e.*, the FSS or CAA case.

6.1 Current expansion on patches

Equations (C.2) and (C.7) relate the tangential electric fields and current distributions at the screens and the excitation of the entire structure. This section shows how the current distributions on the screens can be found by expansions of the currents on the screens in a complete set of expansion functions.

The magnetic field $\boldsymbol{H}(\boldsymbol{\rho}, z_n)$ has a jump discontinuity in z, due to the presence of the resitive patches on the screens, see Appendix B. The jump discontinuity is modelled according to (B.3), and given by

$$\mathbf{J} \cdot \big(\boldsymbol{H}_{xy}(\boldsymbol{\rho}, z_n^+) - \boldsymbol{H}_{xy}(\boldsymbol{\rho}, z_n^-)\big) = \chi Z_n^{-1} \boldsymbol{E}_{xy}(\boldsymbol{\rho}, z_n)$$

where χ is a characteristic function with support on the patches, *i.e.*, it assumes the value 1 on the patches and 0 elsewhere. In the limit $Z_n \to 0$, we obtain the case with PEC patches earlier reported in [21], *i.e.*, $\chi Z_n^{-1} \boldsymbol{E}_{xy}(\boldsymbol{\rho}, z_n) \to \boldsymbol{J}_S(\boldsymbol{\rho}, z_n)$, when $Z_n \to 0$, where $\boldsymbol{J}_S(\boldsymbol{\rho}, z_n)$ is the induced surface currents on the metallic parts of the sheets, see (B.4).

Assume that $Z_n \neq 0$, and denote $\chi Z_n^{-1} \boldsymbol{E}_{xy}(\boldsymbol{\rho}, z_n) = \boldsymbol{J}_S(\boldsymbol{\rho}, z_n)$. The fact that the lateral electric field is continuous, then implies that the impedance boundary condition can be written

$$\chi \boldsymbol{E}_{xy}(\boldsymbol{\rho}, z_n^-) = \chi \boldsymbol{E}_{xy}(\boldsymbol{\rho}, z_n^+) = Z_n \boldsymbol{J}_S(\boldsymbol{\rho}, z_n) \tag{6.1}$$

The current distributions on the screens are expanded in a complete set of basis functions in order to employ the Galerkin method *i.e.*,

$$\boldsymbol{J}_S(\boldsymbol{\rho}, z_n) = \sum_l \beta_l(z_n) \boldsymbol{j}_l(\boldsymbol{\rho}, z_n) \quad \text{on the resistive parts of } S_n$$

where l is a typically multi-index. Employing the Galerkin method, we furthermore define the following vector-valued weight functions

$$\boldsymbol{w}_k(\boldsymbol{\rho}, z_n) = \begin{cases} \mathbf{0} & \text{outside the resistive parts of } S_n \\ \boldsymbol{j}_k(\boldsymbol{\rho}, z_n) & \text{on the resistive parts of } S_n \end{cases} \tag{6.2}$$

whith support on the patches of the screen S_n. Application of the Galerkin method on (6.1) gives

$$\iint_{-\infty}^{\infty} \boldsymbol{w}_k(\boldsymbol{\rho}, z_n)^* \cdot \boldsymbol{E}_{xy}(\boldsymbol{\rho}, z_n)\, dx\, dy = Z_n \iint_{-\infty}^{\infty} \boldsymbol{w}_k(\boldsymbol{\rho}, z_n)^* \cdot \boldsymbol{J}_S(\boldsymbol{\rho}, z_n)\, dx\, dy$$

and by using the Parseval's theorem we have

$$\iint_{-\infty}^{\infty} \boldsymbol{w}_k(\boldsymbol{k}_t, z_n)^* \cdot \boldsymbol{E}_{xy}(\boldsymbol{k}_t, z_n)\, dk_x\, dk_y = Z_n \iint_{-\infty}^{\infty} \boldsymbol{w}_k(\boldsymbol{k}_t, z_n)^* \cdot \boldsymbol{J}_S(\boldsymbol{k}_t, z_n)\, dk_x\, dk_y \quad (6.3)$$

for $n = 1, \cdots, N$, and all multi-index k, where $\boldsymbol{w}_k(\boldsymbol{k}_t, z_n)$ is the lateral Fourier transform of (6.2). In case of general anisotropic thin sheets, the corresponding identities read

$$\iint_{-\infty}^{\infty} \boldsymbol{w}_k(\boldsymbol{k}_t, z_n)^* \cdot \boldsymbol{E}_{xy}(\boldsymbol{k}_t, z_n)\, dk_x\, dk_y = \iint_{-\infty}^{\infty} \boldsymbol{w}_k(\boldsymbol{k}_t, z_n)^* \cdot \mathbf{Z}_{n2} \cdot \boldsymbol{J}_S(\boldsymbol{k}_t, z_n)\, dk_x\, dk_y \quad (6.4)$$

where the impedance dyadic $\mathbf{Z}_{n2}$ is a linear map $\mathbb{C}^2 \to \mathbb{C}^2$ modelling the more general impedance boundary conditions

$$\boldsymbol{E}_{xy}(\boldsymbol{\rho}, z_n^-) = \boldsymbol{E}_{xy}(\boldsymbol{\rho}, z_n^+) = \mathbf{Z}_{n2} \cdot \chi \boldsymbol{J}_S(\boldsymbol{\rho}, z_n) \quad (6.5)$$

The lateral electric fields vanish on the metallic parts of the sheets in the metallic case, which also is seen in the limit $Z_n \to 0$ ($\mathbf{Z}_{n2} \to \mathbf{0}$) for $n = 1, \cdots, N$ in (6.1) (or (6.5)). Thus, in the limit the identities (6.3) and (6.4) become

$$\iint_{-\infty}^{\infty} \boldsymbol{w}_k(\boldsymbol{k}_t, z_n)^* \cdot \boldsymbol{E}_{xy}(\boldsymbol{k}_t, z_n)\, dk_x\, dk_y = 0, \quad \mathbf{Z}_{n2} \to \mathbf{0}$$

for $n = 1, \cdots, N$, which is identical with the corresponding result reported in [21].

Equation (C.2) or (C.7) can now be substituted in either (6.3) or (6.4) to find the unknowns $\beta_l(z_n)$. For more than one sheet, *i.e.*, $N > 1$, we obtain

$$\begin{aligned}\sum_l \sum_{m=1}^{N} b_{nklm} \beta_l(z_n) = \\ \iint_{-\infty}^{\infty} \boldsymbol{w}_k(\boldsymbol{k}_t, z_n)^* \cdot \mathbf{B}_{n0}(\boldsymbol{k}_t) \cdot \boldsymbol{F}^+(\boldsymbol{k}_t, z_0)\, dk_x\, dk_y \\ + \iint_{-\infty}^{\infty} \boldsymbol{w}_k(\boldsymbol{k}_t, z_n)^* \cdot \mathbf{B}_{nN+1}(\boldsymbol{k}_t) \cdot \boldsymbol{F}^-(\boldsymbol{k}_t, z_{N+1})\, dk_x\, dk_y\end{aligned}$$

for $n = 1, \cdots, N$, and all multi-index k where

$$b_{nklm} = \eta_0 \iint_{-\infty}^{\infty} \boldsymbol{w}_k(\boldsymbol{k}_t, z_n)^* \cdot \left(\mathbf{B}_{nm}(\boldsymbol{k}_t) \cdot \boldsymbol{j}_l(\boldsymbol{k}_t, z_m) - \delta_{mn} \frac{Z_n}{\eta_0} \boldsymbol{j}_l(\boldsymbol{k}_t, z_n) \right) dk_x\, dk_y$$

or in the general case of anisotropic resistive sheets

$$b_{nklm} = \eta_0 \iint_{-\infty}^{\infty} \boldsymbol{w}_k(\boldsymbol{k}_t, z_n)^* \cdot \left(\mathbf{B}_{nm}(\boldsymbol{k}_t) \cdot \boldsymbol{j}_l(\boldsymbol{k}_t, z_m) - \frac{\delta_{mn}}{\eta_0} \mathbf{Z}_{n2} \cdot \boldsymbol{j}_l(\boldsymbol{k}_t, z_n) \right) dk_x\, dk_y$$

6.2 Current expansion on periodic patches

As in Section 6.1 we expand the current density $\boldsymbol{J}_S(\boldsymbol{\rho}, z_j)$ in a complete set of entire domain or local basis functions, but due to the periodicity it suffices to define the basis functions in the unit cell U [21].

Expand the current density $\boldsymbol{J}_S(\boldsymbol{\rho}, z_j)$ according to

$$\boldsymbol{J}_S(\boldsymbol{\rho}, z_j) = \sum_{p\in\Lambda} C_p^j \boldsymbol{j}_p(\boldsymbol{\rho}, z_j), \qquad j = 1, 2, \ldots, N;\ \boldsymbol{\rho} \in U$$

where Λ is a countable set of indices and, the scalars C_p^j, the unknown expansion coefficients. The lateral Fourier transform of the current expansion is [21]

$$\boldsymbol{J}_S|_U(\boldsymbol{k}_{mn}, z_j) = \sum_{p\in\Lambda} C_p^j \boldsymbol{j}_p(\boldsymbol{k}_{mn}, z_j), \qquad j = 1, 2, \ldots, N \tag{6.6}$$

where

$$\boldsymbol{j}_p(\boldsymbol{k}_{mn}, z_j) = \iint\limits_U \boldsymbol{j}_p(\boldsymbol{\rho}, z_j) e^{-i\boldsymbol{k}_{mn}\cdot\boldsymbol{\rho}} dxdy, \qquad j = 1, 2, \ldots, N;\ p \in \Lambda$$

In analogy with Section 6.1, we make use of weigth functions, $\boldsymbol{w}_p(\boldsymbol{\rho}, z_j)$, supported on the patches *i.e.*, (6.2) with lateral Fourier transforms defined by

$$\boldsymbol{w}_p(\boldsymbol{k}_{mn}, z_j) = \iint\limits_U \boldsymbol{w}_p(\boldsymbol{\rho}, z_j) e^{-i\boldsymbol{k}_{mn}\cdot\boldsymbol{\rho}} dxdy, \qquad j = 1, 2, \ldots, N;\ p \in \Lambda$$

From the impedance boundary condition (6.1), we have the following identity

$$\iint\limits_U \boldsymbol{w}_p(\boldsymbol{\rho}, z_j)^* \cdot \boldsymbol{E}_{xy}(\boldsymbol{\rho}, z_j)\, dx\, dy = Z_j \iint\limits_U \boldsymbol{w}_p(\boldsymbol{\rho}, z_j)^* \cdot \boldsymbol{J}_S(\boldsymbol{\rho}, z_j)\, dx\, dy$$

for $j = 1, 2, \ldots, N;\ p \in \Lambda$. By the use of the Parseval's theorem for Fourier series[5] modified to Floquet expansions[6], the identity can be written as

$$\sum_{m,n=-\infty}^{\infty} \boldsymbol{w}_p(\boldsymbol{k}_{mn}, z_j)^* \cdot \boldsymbol{E}_{xy}|_U(\boldsymbol{k}_{mn}, z_j) = Z_j \sum_{m,n=-\infty}^{\infty} \boldsymbol{w}_p(\boldsymbol{k}_{mn}, z_j)^* \cdot \boldsymbol{J}_S|_U(\boldsymbol{k}_{mn}, z_j)$$

---

[5] If f and g are doubly periodic functions in $\boldsymbol{\rho} \in \mathbb{R}^2$ with unit cell $U = \{\boldsymbol{a}s + \boldsymbol{b}t\colon 0 \le s, t \le 1\}$, defined by the linearly independent vectors $\boldsymbol{a} \in \mathbb{R}^2$ and $\boldsymbol{b} \in \mathbb{R}^2$, and the Fourier coefficients of f and g are f_{mn} and g_{mn}, respectively, Parseval's theorem is given by [21]:

$$\frac{1}{A_U} \iint\limits_U f^*(\boldsymbol{\rho}) g(\boldsymbol{\rho}) dxdy = \sum_{m,n=-\infty}^{\infty} f_{mn}^* g_{mn}$$

where the area of the unit cell U is $A_U = |\hat{\boldsymbol{z}} \cdot (\boldsymbol{a} \times \boldsymbol{b})|$.

[6] By an application of the Floquet's theorem to the induced surface currents at the periodic screens, the current densities have the Fourier series representation [21]

$$\boldsymbol{J}_S(\boldsymbol{\rho}, z_j) = \frac{1}{A_U} \sum_{m,n=-\infty}^{\infty} \boldsymbol{J}_S|_U(\boldsymbol{k}_{mn}, z_j) e^{i\boldsymbol{k}_{mn}\cdot\boldsymbol{\rho}} \qquad j = 1, 2, \ldots, N;\ \boldsymbol{\rho} \in \mathbb{R}$$

A similar Floquet expansion exists for the lateral electric field $\boldsymbol{E}_{xy}(\boldsymbol{\rho}, z_j)$.

for $j = 1, 2, \ldots, N;\ p \in \Lambda$, in which equation[7] (C.12) and, the lateral Fourier transform of the current expansion (6.6) are substituted, which yields a system of equations for the unknown coefficients C_p^j *i.e.*,

$$\begin{aligned}\sum_{m,n=-\infty}^{\infty} \boldsymbol{w}_p(\boldsymbol{k}_{mn}, z_j)^* \cdot \left(\sum_{k=1}^{N} \mathbf{B}_{jk}(\boldsymbol{k}_{mn}) - \frac{Z_j}{\eta_0} \delta_{jk} \mathbf{I}_2 \right) \cdot \eta_0 \sum_{q \in \chi} C_q^k \boldsymbol{j}_q(\boldsymbol{k}_{mn}, z_k) \\ = A_U \boldsymbol{w}_p(\boldsymbol{k}_{00}, z_j)^* \cdot \mathbf{B}_{j0}(\boldsymbol{k}_{00}) \cdot \boldsymbol{F}^+(\boldsymbol{k}_{00}, z_0), \qquad j = 1, 2, \ldots, N;\ p \in \Lambda\end{aligned} \tag{6.7}$$

Letting $Z_j \to 0$ for $j = 1, \cdots, N$ in (6.7), we obtain

$$\begin{aligned}\sum_{m,n=-\infty}^{\infty} \boldsymbol{w}_p(\boldsymbol{k}_{mn}, z_j)^* \cdot \sum_{k=1}^{N} \mathbf{B}_{jk}(\boldsymbol{k}_{mn}) \cdot \eta_0 \sum_{q \in \chi} C_q^k \boldsymbol{j}_q(\boldsymbol{k}_{mn}, z_k) \\ = A_U \boldsymbol{w}_p(\boldsymbol{k}_{00}, z_j)^* \cdot \mathbf{B}_{j0}(\boldsymbol{k}_{00}) \cdot \boldsymbol{F}^+(\boldsymbol{k}_{00}, z_0), \qquad j = 1, 2, \ldots, N;\ p \in \Lambda\end{aligned} \tag{6.8}$$

which is identical to the corresponding result for the metallic case reported in [21].

The identities (6.7) and (6.8) are infinite systems of linear equations for the unknown current coefficients C_q^k. After truncation they can be written in the form

$$\mathbf{A}\boldsymbol{C} = \boldsymbol{b}$$

where $\mathbf{A}$ is a square matrix, $\boldsymbol{C}$ is a vector containing the unknown coefficients C_q^k, and $\boldsymbol{b}$ is a known vector. The matrix elements for the resistive case are

$$\begin{aligned}A_{jp,kq} = \sum_{m,n=-\infty}^{\infty} \boldsymbol{w}_p(\boldsymbol{k}_{mn}, z_j)^* \cdot (\eta_0 \mathbf{B}_{jk}(\boldsymbol{k}_{mn}) - Z_j \delta_{jk} \mathbf{I}_2) \cdot \boldsymbol{j}_q(\boldsymbol{k}_{mn}, z_k) \\ j, k = 1, 2, \ldots, N;\ p, q \in \Lambda\end{aligned}$$

or in case of anisotropic resistive sheets the elements are

$$\begin{aligned}A_{jp,kq} = \sum_{m,n=-\infty}^{\infty} \boldsymbol{w}_p(\boldsymbol{k}_{mn}, z_j)^* \cdot (\eta_0 \mathbf{B}_{jk}(\boldsymbol{k}_{mn}) - \delta_{jk} \mathbf{Z}_{j2}) \cdot \boldsymbol{j}_q(\boldsymbol{k}_{mn}, z_k) \\ j, k = 1, 2, \ldots, N;\ p, q \in \Lambda\end{aligned}$$

where the impedance dyadic $\mathbf{Z}_{j2}$ is a linear map $\mathbb{C}^2 \to \mathbb{C}^2$ in analogy with the results in Section 6.1. Furthermore, the elements of the right-hand side $\boldsymbol{b}$ are given by

$$b_{jp} = A_U \boldsymbol{w}_p(\boldsymbol{k}_{00}, z_j)^* \cdot \mathbf{B}_{j0}(\boldsymbol{k}_{00}) \cdot \boldsymbol{F}^+(\boldsymbol{k}_{00}, z_0), \qquad j = 1, 2, \ldots, N;\ p \in \Lambda$$

The theory for computations of reflection and transmission coefficients from the results reported in this section can be found in [21].

[7] In case of one screen is (C.11) substituded.

7 Numerical examples

This section presents some numerical examples, where comparison to data presented in the litterature as well as measured data are shown. The frequency response of the classical Salisbury and Jaumann absorbers consisting of one or several homogeneous resistive sheets is first shown, and secondly the frequency response from two examples with sheets constituting of periodic resistive patches of square patch and crossed dipole type, respectively.

7.1 Absorbers (Salisbury and Jaumann)

In Section 5, it was shown how the propagator formalism could be modified to thin resistive sheets by the use of an approximative boundary condition. The method has been verified against data presented in [25] and [17], respectively, where examples of frequency response of Salisbury and Jaumann absorbers are shown.

Figure 5 and 6 show the frequency response of a Salisbury and a Jaumann absorber, respectively, computed by the propagator formalism presented in Section 5 and the corresponding results from [25] and [17] obtained by the *PMM program (periodic method of moments)* and *CST Microwave studio*, respectively. As seen both in Figure 5 and 6 the agreement is excellent.

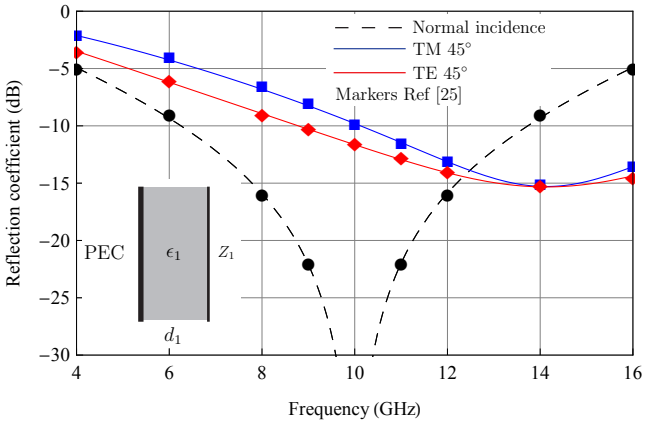

Figure 5: The frequency response of a Salisbury absorber for normal and oblique angles of incidence 45°. Design parameters, $\epsilon_1 = 1.00$, $d_1 = 7.50$, and $Z_1 = 377$ where ϵ denotes the relative permittivity, d layer thickness in (mm), and Z surface resistivity in (Ω/Sq).

In the examples above, it was assumed that the supporting slabs where isotropic and thus modelled by the constitutive relations (2.4) in Section 2. However the propagator method can handle general bianisotropic materials [29], and one interesting question is to investigate what impact the use of uniaxial materials has on the frequency response for a given absorber design. Examples of uniaxial materials in practice are core materials such that Honey comb with a given cell structure and

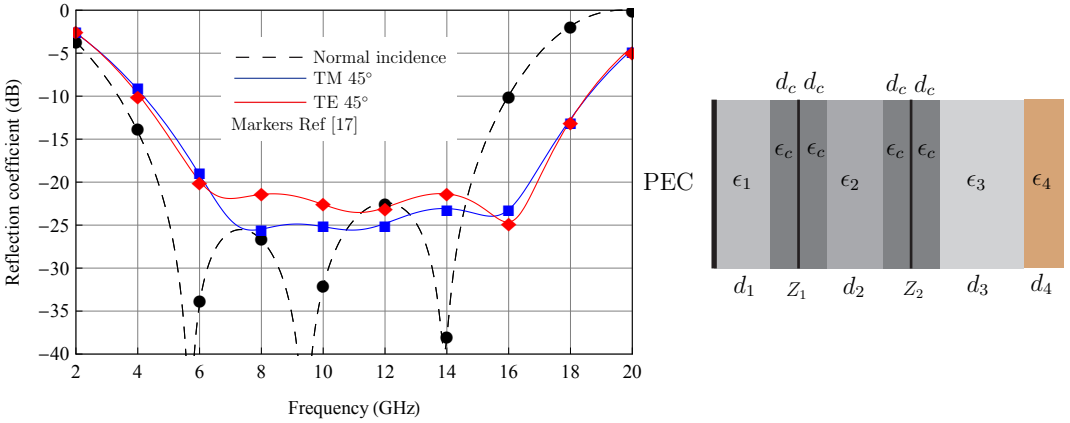

Figure 6: The frequency response of the Jaumann absorber for normal and oblique angles of incidence 45°. Design parameters, $\epsilon_1 = 1.80$, $\epsilon_2 = 1.90$, $\epsilon_3 = 1.30$, $\epsilon_4 = 3.00$, $\epsilon_c = 3.20$, $d_1 = 5.50$, $d_2 = 5.10$, $d_3 = 4.00$, $d_4 = 0.76$, $d_c = 0.20$ and $Z_1 = 196$, $Z_2 = 710$, where ϵ denotes the relative permittivity, d layer thickness in (mm), and Z surface resistivity in (Ω/Sq).

woven materials *e.g.*, fiber reinforced composites, [28]. The constitutive relations for a general uniaxial material are given by (2.3) in Section 2 where

$$\boldsymbol{\epsilon} = \begin{pmatrix} \epsilon_{xx} & 0 & 0 \\ 0 & \epsilon_{yy} & 0 \\ 0 & 0 & \epsilon_{zz} \end{pmatrix} \qquad \boldsymbol{\mu} = \begin{pmatrix} \mu_{xx} & 0 & 0 \\ 0 & \mu_{yy} & 0 \\ 0 & 0 & \mu_{zz} \end{pmatrix} \tag{7.1}$$

and $\epsilon_{xx} = \epsilon_{yy} \neq \epsilon_{zz}$ and/or $\mu_{xx} = \mu_{yy} \neq \mu_{zz}$.

Figure 7 presents the frequency response of the Jaumann absorber in Figure 6, where some of the isotropic layers have been replaced by uniaxial layers according to (7.1) with the exception that the layers are assumed to be non-magnetic *i.e.*, $\mu_{xx} = \mu_{yy} = \mu_{zz} = 1$, see Figure 7 for details. Figure 7 shows that the introduction of uniaxial non-magnetic layers with consitutive relations where $\epsilon_{xx} = \epsilon_{yy} \neq \epsilon_{zz}$ only affect the frequency response of the TM polarization for oblique angle of incidence. This result is physicaly resonable, due to the fact that the uniaxial direction was choosen normal to the interface of the structure, see (7.1). The opposite change by letting $\epsilon_{xx} = \epsilon_{yy} = \epsilon_{zz}$ and $\mu_{xx} = \mu_{yy} \neq \mu_{zz}$ will only affect the TE polarization for oblique angle of incidence, and leave the frequency response of the TM polarization unchanged.

7.2 Resistive periodic structures (Patch and Crossed dipoles)

This section presents results of frequency response from free-standing periodic arrays of perfectly conducting and resistive (lossy) patches as well as resistive crossed dipoles on a flat printed circuit board (PCB). The frequency response from the arrays was computed by the Galerkin method presented in Section 6.2. The results

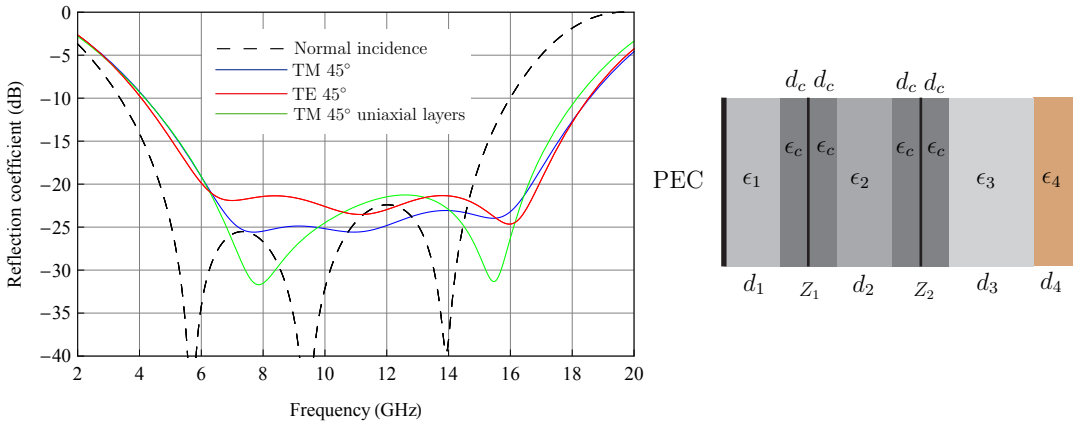

Figure 7: The frequency response of two Jaumann absorbers (i) design in Figure 6 and (ii), where ϵ_i, $i = 1, 2, 3, 4$ in Figure 6 have been replaced with uniaxial material parameters given by $\epsilon_{1xx} = \epsilon_{1yy} = 1.80$, $\epsilon_{1zz} = 2.00$, $\epsilon_{2xx} = \epsilon_{2yy} = 1.90$, $\epsilon_{2zz} = 2.10$, $\epsilon_{3xx} = \epsilon_{3yy} = 1.30$, $\epsilon_{3zz} = 1.50$, $\epsilon_{4xx} = \epsilon_{4yy} = 3.00$, $\epsilon_{4zz} = 3.20$.

for the patch cases are compared with corresponding results found in [9] and the crossed dipole case is compared against measured data.

Patch case The method presented in [9] is a fast Fourier transform-based (FFT) iterative approach for computing the scattered fields from an infinite, periodic array where in general the elements can be perfectly conducting or lossy. The approach in [9] uses subdomain expansion functions in contrast to the method in this paper, which uses entire domain basis functions for the patches according to [19]. Figure 8 shows good agreement between results computed by the method in this paper and the approach in [9].

Crossed dipole case The improved set of entire domain basis functions for the crossed dipoles presented in [26] has been used in the numerical computations of the crossed dipole case. Figure 9 shows a comparison between measured and corresponding computed transmission loss of a flat PCB constituting of a periodic array of resistive crossed dipoles. The PCB has been modelled by a homogeneous isotropic slab *i.e.*, the constitutive relations (2.4) with thickness 0.13 (mm) where the relative permittivity and loss tangent values where set to $\epsilon = 5.40$ and $\tan\delta = 0.0135$ respectively. It is seen in Figure 9 that there is good agreement between measured and computed results.

8 Conclusions

The theory in this paper is based on the concept of propagators to solve scattering problems in planar geometries with an arbitrary number of metallic or resistive

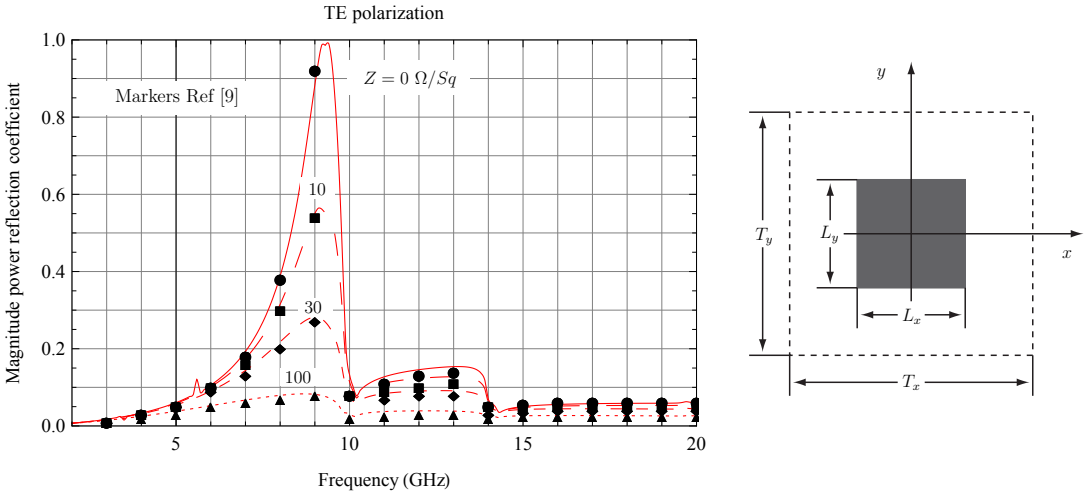

Figure 8: Frequency response of a periodic array of resistive patches for TE incidence at angles of incidence $\theta_i = \phi_i = 1.0°$. The design parameters are the period $T_x = T_y = 30.0$ and the patch width and height $L_x = L_y = 15.0$ given in (mm) with surface resistivity $Z = 0$, 10, 30 and 100 (Ω/Sq) respectively. The curves in each case where computed with $(2 \cdot 8 + 1)^2$ Floquet modes and 12 entire domain basis functions [19].

sheets imbedded in supporting slabs, where the materials in the slabs can be arbitrary linear materials, *i.e.*, a bianisotropic materials.

The paper presents a generalisation of the method of propagators given in [29], where thin homogeneous, in general, anisotropic resistive sheets were modelled by the use of an approximative impedance boundary condition, [9, 12, 15, 31]. Numerical computations has been compared with corresponding results from [25] and [17] obtained by the *PMM program (periodic method of moments)* and *CST Microwave studio*, respectively, with excellent agreement.

The paper has also considered a generalization of the propagator method given in [21] by extending the method to periodic structures with resistive patch type elements. Results from numerical computations were compared with corresponding results from [9] with good agreement. In a final example a comparison between measured and simulated data for the case of an array of resistive crossed dipoles printed on a flat PCB was presented. The improved set of entire domain basis functions presented in [26] was used in the simulations with good agreement between measured and computed data.

Acknowledgments

I am grateful to prof. Gerhard Kristensson and Dr. Sören Poulsen for their support throughout this work. Dr. Björn Widenberg is also gratituded for providing measured data. The work reported in this paper was supported by grants from the

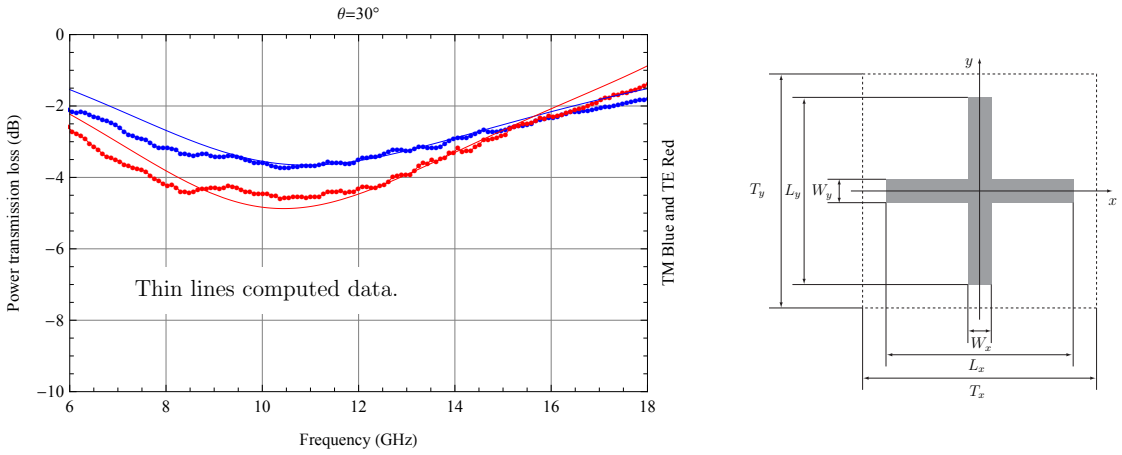

Figure 9: Frequency response of a periodic array of resistive crossed dipoles for TM and TE incidence at angles of incidence $\theta_i = 30.0°$ ($\phi_i = 0.0°$). The design parameters are the period $T_x = T_y = 10.4$ with dipole dimensions $W_x = W_y = 1.0$ and $L_x = L_y = 10.2$ given in (mm) with surface resistivity $Z = 25$ (Ω/Sq) respectively. The PCB was attached on one side to the dipole array with thickness 0.13 (mm) and relative permittivity and loss tangent values set to $\epsilon = 5.40$ and $\tan\delta = 0.0135$ respectively. The curves in each case were computed with $(2\cdot 20+1)^2$ Floquet modes and 16 entire domain basis functions [26].

Swedish Defence Materiel Administration (FMV), which is gratefully acknowledged.

Appendix A Cayley-Hamilton theorem

The following theorems are of fundamental importance for computing the action of an entire function of a square dyadic [6].

Theorem A.1 (Cayley-Hamilton)**.** *A quadratic dyadic* $\mathbf{A}$ *satisfies its own characteristic equation:*

$$\textit{If } p_{\mathbf{A}}(\lambda) = \det(\lambda\mathbf{I} - \mathbf{A}), \textit{ then } p_{\mathbf{A}}(\mathbf{A}) = \mathbf{0}$$

From this theorem, one can prove the following important theorem.

Theorem A.2. *Let* $\lambda_1, \ldots, \lambda_m$ *be the different eigenvalues of the* n*-dimensional dyadic* $\mathbf{A}$*, and* $n_1, \ldots, n_m$ *their multiplicity. If* $f(z)$ *is an entire function, then*

$$f(\mathbf{A}) = q(\mathbf{A})$$

where the uniquely defined polynomial q *of degree* $\leq n-1$ *is defined by the following conditions:*

$$\frac{d^j q}{dz^j}(\lambda_k) = \frac{d^j f}{dz^j}(\lambda_k), \qquad j = 0, \ldots, n_k - 1, k = 1, \ldots, m$$

I: Dielectric boundary

ϵ_1	$\boldsymbol{E}_{xy1}(\boldsymbol{\rho}, z_k)$	$\eta_0 \mathbf{J} \cdot \boldsymbol{H}_{xy1}(\boldsymbol{\rho}, z_k)$	$z = z_k$
ϵ_2	$\boldsymbol{E}_{xy2}(\boldsymbol{\rho}, z_k)$	$\eta_0 \mathbf{J} \cdot \boldsymbol{H}_{xy2}(\boldsymbol{\rho}, z_k)$	

II: Homogeneous impedance boundary

ϵ_1	$\boldsymbol{E}_{xy1}(\boldsymbol{\rho}, z_k)$	Z_k	$\eta_0 \mathbf{J} \cdot \boldsymbol{H}_{xy1}(\boldsymbol{\rho}, z_k)$	$z = z_k$
ϵ_2	$\boldsymbol{E}_{xy2}(\boldsymbol{\rho}, z_k)$	$\eta_0 \mathbf{J} \cdot \boldsymbol{H}_{xy2}(\boldsymbol{\rho}, z_k) + \eta_0 Z_k^{-1} \boldsymbol{E}_{xy2}(\boldsymbol{\rho}, z_k)$		

III: Dielectric boundary with resistive patches

ϵ_1	$\boldsymbol{E}_{xy1}(\boldsymbol{\rho}, z_k)$	Z_k	$\eta_0 \mathbf{J} \cdot \boldsymbol{H}_{xy1}(\boldsymbol{\rho}, z_k)$	$z = z_k$
ϵ_2	$\boldsymbol{E}_{xy2}(\boldsymbol{\rho}, z_k)$	$\eta_0 \mathbf{J} \cdot \boldsymbol{H}_{xy2}(\boldsymbol{\rho}, z_k) + \eta_0 \chi Z_k^{-1} \boldsymbol{E}_{xy2}(\boldsymbol{\rho}, z_k)$		

Figure 10: Different boundaries at the planar interface, $z = z_k$. Case I: Dielectric boundary, Case II: Homogeneous impedance boundary, and Case III: Dielectric boundary with resistive patches.

Appendix B Boundary conditions lateral fields

The foundation of the theory presented in this paper is based on the concept of propagators, which are mappings that relates the total transversal fields between different points in space. A necessary condition for the use of the propagators is that the transversal (lateral) fields are continuous at each boundary, $z = z_k$. Otherwise, one need to employ an appropriate boundary condition, that takes the jump discontinuity into account. The analysis in this paper is not restricted to plane wave incidence by the fact that the fields can be decomposed into a spectrum of plane waves. Due to the planar geometry presented in Section 2, the plane wave decomposition is acomplished by taking the lateral Fourier transform with respect to the lateral position vector $\boldsymbol{\rho} = \hat{\boldsymbol{x}}x + \hat{\boldsymbol{y}}y$, see Section 3. Thus, in order to use the concept of propagators in the Fourier domain, the lateral Fourier transformed fields need to be continuous at each boundary, $z = z_k$, otherwise an appropriate boundary condition is used to model the jump discontinuity.

Boundaries that are considered within the theory of this paper are depicted in Figure 10. Case I in Figure 10 illustrates a pure dielectric boundary at $z = z_k$, where the lateral electric and magnetic fields are continuous, which implies continuity of the corresponding lateral Fourier transformed fields, *i.e.*,

$$\begin{cases} \boldsymbol{E}_{xy1}(\boldsymbol{\rho}, z_k) = \boldsymbol{E}_{xy2}(\boldsymbol{\rho}, z_k) \\ \eta_0 \mathbf{J} \cdot \boldsymbol{H}_{xy1}(\boldsymbol{\rho}, z_k) = \eta_0 \mathbf{J} \cdot \boldsymbol{H}_{xy2}(\boldsymbol{\rho}, z_k) \end{cases} \Rightarrow \begin{cases} \boldsymbol{E}_{xy1}(\boldsymbol{k}_t, z_k) = \boldsymbol{E}_{xy2}(\boldsymbol{k}_t, z_k) \\ \eta_0 \mathbf{J} \cdot \boldsymbol{H}_{xy1}(\boldsymbol{k}_t, z_k) = \eta_0 \mathbf{J} \cdot \boldsymbol{H}_{xy2}(\boldsymbol{k}_t, z_k) \end{cases}$$

By the introduction of a homogeneous resistive sheet with surface resistivity Z_k, at z_k, which in general is complex-valued, we obtain Case II shown in Figure 10. In

case of a homogeneous impedance boundary, we make use of the following impedance boundary condition at z_k, [31]

$$\begin{cases} \boldsymbol{E}_{xy1}(\boldsymbol{\rho}, z_k) = \boldsymbol{E}_{xy2}(\boldsymbol{\rho}, z_k) \\ \eta_0 \mathbf{J} \cdot \boldsymbol{H}_{xy1}(\boldsymbol{\rho}, z_k) = \eta_0 \mathbf{J} \cdot \boldsymbol{H}_{xy2}(\boldsymbol{\rho}, z_k) + \eta_0 Z_k^{-1} \boldsymbol{E}_{xy2}(\boldsymbol{\rho}, z_k) \end{cases} \tag{B.1}$$

Thus, in this case the lateral electric field is continuous, but the magnetic field has a jump discontinuity given by the extra term, $\eta_0 Z_k^{-1} \boldsymbol{E}_{xy2}(\boldsymbol{\rho}, z_k)$, in (B.1). Letting $Z_k \to \infty$, it is seen that the boundary conditions for pure dielectric interfaces, *i.e.*, Case I in Figure 10 is obtained, and in the limit $Z_k \to 0$ the location z_k corresponds to a PEC boundary, where the magnetic field $\boldsymbol{H}_{xy}(\boldsymbol{\rho}, z_k)$ has a jump discontinuity *i.e.*, $Z_k^{-1} \boldsymbol{E}_{xy}(\boldsymbol{\rho}, z_k) \to \boldsymbol{J}_S(\boldsymbol{\rho}, z_k)$ when $Z_k \to 0$, where $\boldsymbol{J}_S(\boldsymbol{\rho}, z_k)$ is the induced surface current on the PEC boundary. Taking the lateral Fourier transform of (B.1), implies

$$\begin{cases} \boldsymbol{E}_{xy1}(\boldsymbol{k}_t, z_k) = \boldsymbol{E}_{xy2}(\boldsymbol{k}_t, z_k) \\ \eta_0 \mathbf{J} \cdot \boldsymbol{H}_{xy1}(\boldsymbol{k}_t, z_k) = \eta_0 \mathbf{J} \cdot \boldsymbol{H}_{xy2}(\boldsymbol{k}_t, z_k) + \eta_0 Z_k^{-1} \boldsymbol{E}_{xy2}(\boldsymbol{k}_t, z_k) \end{cases} \tag{B.2}$$

The boundary condition (B.2) is used when mapping the fields through the thinn homogeneous impedance sheet at $z = z_k$, and the extra term $\eta_0 Z_k^{-1} \boldsymbol{E}_{xy2}(\boldsymbol{k}_t, z_k)$, in (B.2) models the jump discontinuity of the lateral magnetic field.

Case III in Figure 10, *i.e.*, a dielectric boundary with resistive patches, is in fact a combination of the two former boundaries. In this case, the extra term $\eta_0 Z_k^{-1} \boldsymbol{E}_{xy2}(\boldsymbol{\rho}, z_k)$ in (B.1) has compact support on the patches, and, thus, the boundary condition is changed according to

$$\begin{cases} \boldsymbol{E}_{xy1}(\boldsymbol{\rho}, z_k) = \boldsymbol{E}_{xy2}(\boldsymbol{\rho}, z_k) \\ \eta_0 \mathbf{J} \cdot \boldsymbol{H}_{xy1}(\boldsymbol{\rho}, z_k) = \eta_0 \mathbf{J} \cdot \boldsymbol{H}_{xy2}(\boldsymbol{\rho}, z_k) + \eta_0 \chi Z_k^{-1} \boldsymbol{E}_{xy2}(\boldsymbol{\rho}, z_k) \end{cases} \tag{B.3}$$

where χ, is a characteristic function of the patches, *i.e.*, it assumes the value 1 on the patches and 0 elsewhere.

Notice that, $\chi Z_k^{-1} \boldsymbol{E}_{xy}(\boldsymbol{\rho}, z_k) \to \boldsymbol{J}_S(\boldsymbol{\rho}, z_k)$, in the limit $Z_k \to 0$, which corresponds to the case with PEC patches earlier reported in [21] *i.e.*,

$$\begin{cases} \boldsymbol{E}_{xy1}(\boldsymbol{\rho}, z_k) = \boldsymbol{E}_{xy2}(\boldsymbol{\rho}, z_k) \\ \boldsymbol{J}_S(\boldsymbol{\rho}, z_k) = \eta_0 \mathbf{J} \cdot (\boldsymbol{H}_{xy1}(\boldsymbol{\rho}, z_k) - \boldsymbol{H}_{xy2}(\boldsymbol{\rho}, z_k)) \end{cases} \tag{B.4}$$

Appendix C Current and lateral field relations

To solve the scattering problem for a structure consisting of one or several screens depicted in Figure 1 with apertures or patches, one needs expressions for the current distributions or tangential electric fields at the screens. The analysis presented in [21] formulates those relations by the propagator formalism separated into two paths, depending on whether there are one screen ($N = 1$), or whether there are several screens ($N > 1$). These cases are different due, to the fact that in the first case the

screen has the two half spaces next to the screen, and in the second case there is always a neighboring screen.

This appendix summarizes the relations derived in [21] between the surface currents, $\boldsymbol{J}_S(\boldsymbol{k}_t, z_n)$, on the screens and electric fields, $\boldsymbol{E}_{xy}(\boldsymbol{k}_t, z_n)$, on the screens and excitations of the entire slab, denoted by $\boldsymbol{F}^+(\boldsymbol{k}_t, z_0)$ and $\boldsymbol{F}^-(\boldsymbol{k}_t, z_{N+1})$, *i.e.*, the excitations from the left and right, respectively.

C.1 Relations in the non-periodic case

One screen ($N = 1$): For the case of only one screen it is found in [21] that

$$\begin{aligned}\eta_0 \boldsymbol{J}_S(\boldsymbol{k}_t, z_1) =& \mathbf{A}_{11}(\boldsymbol{k}_t) \cdot \boldsymbol{E}_{xy}(\boldsymbol{k}_t, z_1) \\ &+ \mathbf{A}_{10}(\boldsymbol{k}_t) \cdot \boldsymbol{F}^+(\boldsymbol{k}_t, z_0) + \mathbf{A}_{12}(\boldsymbol{k}_t) \cdot \boldsymbol{F}^-(\boldsymbol{k}_t, z_2)\end{aligned} \tag{C.1}$$

where[8] the square (2×2) matrices $\mathbf{A}_{nm}(\boldsymbol{k}_t)$, $n = 1$ and $m = 0, 1, 2$ are

$$\begin{cases} \boldsymbol{A}_{10}(\boldsymbol{k}_t) = -2(\mathbf{P}_{em} - \mathbf{W} \cdot \mathbf{P}_{mm})^{-1}(\boldsymbol{k}_t, z_0, z_1) \\ \mathbf{A}_{11}(\boldsymbol{k}_t) = -((\mathbf{P}_{em} + \mathbf{W} \cdot \mathbf{P}_{mm})^{-1} \cdot (\mathbf{P}_{ee} + \mathbf{W} \cdot \mathbf{P}_{me}))(\boldsymbol{k}_t, z_2, z_1) \\ \qquad\qquad + ((\mathbf{P}_{em} - \mathbf{W} \cdot \mathbf{P}_{mm})^{-1} \cdot (\mathbf{P}_{ee} - \mathbf{W} \cdot \mathbf{P}_{me}))(\boldsymbol{k}_t, z_0, z_1) \\ \mathbf{A}_{12}(\boldsymbol{k}_t) = 2(\mathbf{P}_{em} + \mathbf{W} \cdot \mathbf{P}_{mm})^{-1}(\boldsymbol{k}_t, z_2, z_1) \end{cases}$$

The dyadics $\mathbf{P}_{ee}$, $\mathbf{P}_{em}$, $\mathbf{P}_{me}$ and $\mathbf{P}_{mm}$ denotes block dyadics of the propagators $\mathbf{P}(\boldsymbol{k}_t, z_0, z_1)$ and $\mathbf{P}(\boldsymbol{k}_t, z_2, z_1)$, and $\mathbf{W}$ is given by

$$\begin{aligned}\mathbf{W}(\boldsymbol{k}_t) =& \frac{k_z}{k_0}\left(\mathbf{I}_2 - \frac{1}{k_z^2}\boldsymbol{k}_t \times (\boldsymbol{k}_t \times \mathbf{I}_2)\right) = \hat{\boldsymbol{e}}_\parallel \hat{\boldsymbol{e}}_\parallel \frac{k_z}{k_0} + \hat{\boldsymbol{e}}_\perp \hat{\boldsymbol{e}}_\perp \frac{k_0}{k_z} \\ =& \frac{k_0}{k_z}\left(\mathbf{I}_2 - \frac{1}{k_0^2}\boldsymbol{k}_t \boldsymbol{k}_t\right) = \frac{k_0}{k_z}\mathbf{I}_2 - \frac{k_t^2}{k_0 k_z}\hat{\boldsymbol{e}}_\parallel \hat{\boldsymbol{e}}_\parallel\end{aligned}$$

Equation (C.1) is a relation between the surface current, the transverse electric field at the screen, and the excitations of the structure to the left and right respectively. Notice that the screen is assumed to be located in between two slabs with outer boundaries located at z_0 and z_2, respectively.

Relation (C.1) can be inverted, and the transverse electric field $\boldsymbol{E}_{xy}(\boldsymbol{k}_t, z_1)$ can be found in terms of the surface currents $\boldsymbol{J}_S(\boldsymbol{k}_t, z_1)$ according to [21]

$$\begin{aligned}\boldsymbol{E}_{xy}(\boldsymbol{k}_t, z_1) =& \mathbf{B}_{11}(\boldsymbol{k}_t) \cdot \eta_0 \boldsymbol{J}_S(\boldsymbol{k}_t, z_1) \\ &- \mathbf{B}_{10}(\boldsymbol{k}_t) \cdot \boldsymbol{F}^+(\boldsymbol{k}_t, z_0) - \mathbf{B}_{12}(\boldsymbol{k}_t) \cdot \boldsymbol{F}^-(\boldsymbol{k}_t, z_2)\end{aligned} \tag{C.2}$$

where

$$\begin{cases} \mathbf{B}_{11}(\boldsymbol{k}_t) = \mathbf{A}_{11}(\boldsymbol{k}_t)^{-1} \\ \mathbf{B}_{10}(\boldsymbol{k}_t) = \mathbf{B}_{11}(\boldsymbol{k}_t) \cdot \mathbf{A}_{10}(\boldsymbol{k}_t) \\ \mathbf{B}_{12}(\boldsymbol{k}_t) = \mathbf{B}_{11}(\boldsymbol{k}_t) \cdot \mathbf{A}_{12}(\boldsymbol{k}_t) \end{cases}$$

Equation, (C.1), is more adapted for the analysis of the aperture case, while the second one, (C.2), for the patch case [21].

[8] The dependence of the block matrices $\mathbf{A}_{mn}(\boldsymbol{k}_t)$ on the location of the screens are suppressed.

Several screens ($N > 1$): The surface current at the first screen is [21]

$$\begin{aligned}\eta_0 \boldsymbol{J}_S(\boldsymbol{k}_t, z_1) =& \mathbf{A}_{11}(\boldsymbol{k}_t) \cdot \boldsymbol{E}_{xy}(\boldsymbol{k}_t, z_1) + \mathbf{A}_{12}(\boldsymbol{k}_t) \cdot \boldsymbol{E}_{xy}(\boldsymbol{k}_t, z_2) \\ &+ \mathbf{A}_{10}(\boldsymbol{k}_t) \cdot \boldsymbol{F}^+(\boldsymbol{k}_t, z_0)\end{aligned} \tag{C.3}$$

where

$$\begin{cases} \mathbf{A}_{11}(\boldsymbol{k}_t) = (\mathbf{P}_{mm} \cdot \mathbf{P}_{em}^{-1})(\boldsymbol{k}_t, z_1, z_2) \\ \qquad\qquad + ((\mathbf{P}_{em} - \mathbf{W} \cdot \mathbf{P}_{mm})^{-1} \cdot (\mathbf{P}_{ee} - \mathbf{W} \cdot \mathbf{P}_{me}))(\boldsymbol{k}_t, z_0, z_1) \\ \mathbf{A}_{12}(\boldsymbol{k}_t) = (\mathbf{P}_{me} - \mathbf{P}_{mm} \cdot \mathbf{P}_{em}^{-1} \cdot \mathbf{P}_{ee})(\boldsymbol{k}_t, z_1, z_2) \\ \boldsymbol{A}_{10}(\boldsymbol{k}_t) = -2(\mathbf{P}_{em} - \mathbf{W} \cdot \mathbf{P}_{mm})^{-1}(\boldsymbol{k}_t, z_0, z_1) \end{cases}$$

and the surface currents at the interior screens are [21]

$$\begin{aligned}\eta_0 \boldsymbol{J}_S(\boldsymbol{k}_t, z_n) =& \mathbf{A}_{nn-1}(\boldsymbol{k}_t) \cdot \boldsymbol{E}_{xy}(\boldsymbol{k}_t, z_{n-1}) \\ &+ \mathbf{A}_{nn}(\boldsymbol{k}_t) \cdot \boldsymbol{E}_{xy}(\boldsymbol{k}_t, z_n) \qquad (n = 2, \cdots, N-1) \\ &+ \mathbf{A}_{nn+1}(\boldsymbol{k}_t) \cdot \boldsymbol{E}_{xy}(\boldsymbol{k}_t, z_{n+1})\end{aligned} \tag{C.4}$$

where

$$\begin{cases} \mathbf{A}_{nn-1}(\boldsymbol{k}_t) = -\mathbf{P}_{em}^{-1}(\boldsymbol{k}_t, z_{n-1}, z_n) \\ \mathbf{A}_{nn}(\boldsymbol{k}_t) = (\mathbf{P}_{mm} \cdot \mathbf{P}_{em}^{-1})(\boldsymbol{k}_t, z_n, z_{n+1}) + (\mathbf{P}_{em}^{-1} \cdot \mathbf{P}_{ee})(\boldsymbol{k}_t, z_{n-1}, z_n) \\ \mathbf{A}_{nn+1}(\boldsymbol{k}_t) = (\mathbf{P}_{me} - \mathbf{P}_{mm} \cdot \mathbf{P}_{em}^{-1} \cdot \mathbf{P}_{ee})(\boldsymbol{k}_t, z_n, z_{n+1}) \end{cases}$$

Equation (C.4) is a relation between the surface currents and the transverse electric fields at the interior screens and the transverse electric fields at its two neighbors. The surface current on the final screen is [21]

$$\begin{aligned}\eta_0 \boldsymbol{J}_S(\boldsymbol{k}_t, z_N) =& \mathbf{A}_{NN-1}(\boldsymbol{k}_t) \cdot \boldsymbol{E}_{xy}(\boldsymbol{k}_t, z_{N-1}) + \mathbf{A}_{NN}(\boldsymbol{k}_t) \cdot \boldsymbol{E}_{xy}(\boldsymbol{k}_t, z_N) \\ &+ \mathbf{A}_{NN+1}(\boldsymbol{k}_t) \cdot \boldsymbol{F}^-(\boldsymbol{k}_t, z_{N+1})\end{aligned} \tag{C.5}$$

where

$$\begin{cases} \mathbf{A}_{NN-1}(\boldsymbol{k}_t) = -\mathbf{P}_{em}^{-1}(\boldsymbol{k}_t, z_{N-1}, z_N) \\ \mathbf{A}_{NN}(\boldsymbol{k}_t) = (\mathbf{P}_{em}^{-1} \cdot \mathbf{P}_{ee})(\boldsymbol{k}_t, z_{N-1}, z_N) \\ \qquad\qquad - ((\mathbf{P}_{em} + \mathbf{W} \cdot \mathbf{P}_{mm})^{-1} \cdot (\mathbf{P}_{ee} + \mathbf{W} \cdot \mathbf{P}_{me}))(\boldsymbol{k}_t, z_{N+1}, z_N) \\ \mathbf{A}_{NN+1}(\boldsymbol{k}_t) = 2(\mathbf{P}_{em} + \mathbf{W} \cdot \mathbf{P}_{mm})^{-1}(\boldsymbol{k}_t, z_{N+1}, z_N) \end{cases}$$

Combining (C.3), (C.4) and (C.5) into a single expression the relations implies ($n = 1, \cdots, N$), [21]

$$\begin{aligned}\eta_0 \boldsymbol{J}_S(\boldsymbol{k}_t, z_n) =& \sum_{m=1}^{N} \mathbf{A}_{nm}(\boldsymbol{k}_t) \cdot \boldsymbol{E}_{xy}(\boldsymbol{k}_t, z_m) \\ &+ \delta_{n1} \mathbf{A}_{10}(\boldsymbol{k}_t) \cdot \boldsymbol{F}^+(\boldsymbol{k}_t, z_0) + \delta_{nN} \mathbf{A}_{NN+1}(\boldsymbol{k}_t) \cdot \boldsymbol{F}^-(\boldsymbol{k}_t, z_{N+1})\end{aligned} \tag{C.6}$$

where δ denotes the Kronecker delta. Notice that the sum in (C.6) has only at most three terms, since all matrices $\mathbf{A}_{nm}$ vanish if $m \neq n, n \pm 1$. Introducing the square

$(2N \times 2N)$ matrix $\mathbf{A}(\boldsymbol{k}_t) = (\mathbf{A}_{nm}(\boldsymbol{k}_t))$ of band block type in accordiance with the theory in [21] by

$$\mathbf{A} = \begin{pmatrix} \mathbf{A}_{11} & \mathbf{A}_{12} & \mathbf{0} & \dots & \dots & \dots \\ \mathbf{A}_{21} & \mathbf{A}_{22} & \mathbf{A}_{23} & \mathbf{0} & \dots & \dots \\ \mathbf{0} & \mathbf{A}_{32} & \mathbf{A}_{33} & \mathbf{A}_{34} & \mathbf{0} & \dots \\ \vdots & \vdots & \vdots & \ddots & \vdots & \vdots \\ \dots & \dots & \mathbf{0} & \mathbf{A}_{N-1N-2} & \mathbf{A}_{N-1N-1} & \mathbf{A}_{N-1N} \\ \dots & \dots & \dots & \mathbf{0} & \mathbf{A}_{NN-1} & \mathbf{A}_{NN} \end{pmatrix}$$

equation (C.6) can be written in a form adapted for numerical implementation. Similar to (C.2), for the case of only one screen, equation (C.6) can be inverted and the transverse electric field $\boldsymbol{E}_{xy}(\boldsymbol{k}_t, z_n)$ can be found in terms of the surface currents $\boldsymbol{J}_S(\boldsymbol{k}_t, z_m)$, [21]

$$\begin{aligned} \boldsymbol{E}_{xy}(\boldsymbol{k}_t, z_n) = &\sum_{m=1}^{N} \mathbf{B}_{nm}(\boldsymbol{k}_t) \cdot \eta_0 \boldsymbol{J}_S(\boldsymbol{k}_t, z_m) \\ &- \mathbf{B}_{n0}(\boldsymbol{k}_t) \cdot \boldsymbol{F}^{+}(\boldsymbol{k}_t, z_0) - \mathbf{B}_{nN+1}(\boldsymbol{k}_t) \cdot \boldsymbol{F}^{-}(\boldsymbol{k}_t, z_{N+1}) \end{aligned} \tag{C.7}$$

where $\mathbf{B}_{n0}(\boldsymbol{k}_t) := \mathbf{B}_{n1}(\boldsymbol{k}_t) \cdot \mathbf{A}_{10}(\boldsymbol{k}_t)$ and $\mathbf{B}_{nN+1}(\boldsymbol{k}_t) := \mathbf{B}_{nN}(\boldsymbol{k}_t) \cdot \mathbf{A}_{NN+1}(\boldsymbol{k}_t)$.

Equations (C.6) and (C.7) constitute the final set of equations for the case of several screens. The first equation, (C.6), is the most suitable one for the analysis of the aperture case, while the second one, (C.7), is more adapted to the the patch case [21].

C.2 Relations in the periodic case

In FSS or CAA applications, FSS sheets with elements of patch or aperture type arranged in a periodic pattern need to be considered. In case of periodic sheets, it is assumed that the periodicity is the same or commensurate on all screens.

If this is the case, Floquet's theorem [14] can be applied, which implies that the electric fields and the current densities can be expanded in infinite exponential series in terms of lateral wave numbers given by [21]

$$\boldsymbol{k}_{mn} = 2\pi \left(-m \frac{\hat{\boldsymbol{z}} \times \boldsymbol{b}}{\hat{\boldsymbol{z}} \cdot (\boldsymbol{a} \times \boldsymbol{b})} + n \frac{\hat{\boldsymbol{z}} \times \boldsymbol{a}}{\hat{\boldsymbol{z}} \cdot (\boldsymbol{a} \times \boldsymbol{b})} \right) + \boldsymbol{k}_t^i, \qquad m, n \in \mathbb{Z}$$

where $\mathbb{Z}$ denotes the set of integers and $\boldsymbol{a}$ and $\boldsymbol{b}$ denote two linearly independent vectors in the x-y plane, which span the unit cell $U = \{\boldsymbol{a}s + \boldsymbol{b}t \colon 0 \le s, t \le 1\}$ of the periodic sheets. A general result derived in [21] is that the connection between the lateral Fourier transforms of any field quantity, $\boldsymbol{F}_S(\boldsymbol{k}_t, z_j)$, (*e.g.*, the current density and lateral electric field) and the Fourier transform of its restriction to the unit cell, $\boldsymbol{F}_S|_U(\boldsymbol{k}_{mn}, z_j)$, is

$$\boldsymbol{F}_S(\boldsymbol{k}_t, z_j) = \frac{4\pi^2}{A_U} \sum_{m,n=-\infty}^{\infty} \boldsymbol{F}_S|_U(\boldsymbol{k}_{mn}, z_j) \delta^2(\boldsymbol{k}_t - \boldsymbol{k}_{mn}), \qquad j = 1, 2, \dots, N$$

Using this relation for the induced surface current densities, $\boldsymbol{J}_S(\boldsymbol{\rho}, z_j)$, and the lateral electric fields $\boldsymbol{E}_{xy}(\boldsymbol{\rho}, z_j)$ at the screens, gives

$$\boldsymbol{J}_S(\boldsymbol{k}_t, z_j) = \frac{4\pi^2}{A_U} \sum_{m,n=-\infty}^{\infty} \boldsymbol{J}_S|_U(\boldsymbol{k}_{mn}, z_j)\delta^2(\boldsymbol{k}_t - \boldsymbol{k}_{mn}), \qquad j = 1, 2, \ldots, N \quad \text{(C.8)}$$

and

$$\boldsymbol{E}_{xy}(\boldsymbol{k}_t, z_j) = \frac{4\pi^2}{A_U} \sum_{m,n=-\infty}^{\infty} \boldsymbol{E}_{xy}|_U(\boldsymbol{k}_{mn}, z_j)\delta^2(\boldsymbol{k}_t - \boldsymbol{k}_{mn}), \qquad j = 1, 2, \ldots, N \quad \text{(C.9)}$$

where (C.8)–(C.9) are the Fourier transforms of the surface current densities, *i.e.*, $\boldsymbol{J}_S(\boldsymbol{\rho}, z_j)$, and lateral electric fields, $\boldsymbol{E}_{xy}(\boldsymbol{\rho}, z_j)$, respectively at the screens connected to their restrictions to the unit cell.

The results presented in Appendix C.1 was formulated such that there could be sources on both sides of the slab, *i.e.*, in the regions $z < z_0$ and $z > z_{N+1}$. In [21], a plane wave excitation was assumed only from the left and given by

$$\boldsymbol{E}^i(\boldsymbol{r}) = \boldsymbol{E}^i_0 e^{i\boldsymbol{k}^i \cdot \boldsymbol{r}}$$

where $\boldsymbol{k}^i = k_0(\hat{\boldsymbol{x}} \sin\theta\cos\phi + \hat{\boldsymbol{y}} \sin\theta \sin\phi + \hat{\boldsymbol{z}} \cos\theta) = \boldsymbol{k}^i_t + \hat{\boldsymbol{z}} k^i_z$, is the constant real wave vector of the incident wave, where $\boldsymbol{k}^i_t = \mathbf{I}_2 \cdot \boldsymbol{k}^i$ and $k^i_z = \boldsymbol{k}^i \cdot \hat{\boldsymbol{z}}$, and $\boldsymbol{E}^i_0$ is a constant complex vector, such that $\boldsymbol{E}^i_0 \cdot \boldsymbol{k}^i = 0$. In [21], it is, furthermore, shown that the Fourier transform of the lateral part of the excitation can be written

$$\boldsymbol{F}^+(\boldsymbol{k}_t, z_0) = 4\pi^2 \boldsymbol{F}^+(\boldsymbol{k}_{00}, z_0)\delta^2(\boldsymbol{k}_t - \boldsymbol{k}_{00}) \quad \text{(C.10)}$$

where $\boldsymbol{F}^+(\boldsymbol{k}_{00}, z_0) = \boldsymbol{E}^i_{0xy} e^{ik^i_z z_0}$ and $\boldsymbol{k}_{00} = \boldsymbol{k}^i_t$ in accordiance with (C.2) for $m = n = 0$.

By substituting the equations (C.8), (C.9), and (C.10) into relations (C.1) and (C.6) in the aperture case, and relations (C.2) and (C.7) in the patch case, respectively, we get the sought relations in the periodic case.

Aperture case: In case of one screen ($N = 1$) the relation is [21]

$$\begin{aligned}\eta_0 \boldsymbol{J}_S|_U(\boldsymbol{k}_{mn}, z_1) =& \mathbf{A}_{11}(\boldsymbol{k}_{mn}) \cdot \boldsymbol{E}_{xy}|_U(\boldsymbol{k}_{mn}, z_1) \\ &+ A_U \mathbf{A}_{10}(\boldsymbol{k}_{00}) \cdot \boldsymbol{F}^+(\boldsymbol{k}_{00}, z_0)\delta_{m0}\delta_{n0}\end{aligned}$$

and for several screens *i.e.*, $N > 1$, the corresponding relations are [21]

$$\begin{aligned}\eta_0 \boldsymbol{J}_S|_U(\boldsymbol{k}_{mn}, z_j) =& \sum_{k=1}^{N} \mathbf{A}_{jk}(\boldsymbol{k}_{mn}) \cdot \boldsymbol{E}_{xy}|_U(\boldsymbol{k}_{mn}, z_k) \\ &+ A_U \mathbf{A}_{j0}(\boldsymbol{k}_{00}) \cdot \boldsymbol{F}^+(\boldsymbol{k}_{00}, z_0)\delta_{m0}\delta_{n0}\delta_{j1}, \qquad j = 1, 2, \ldots, N\end{aligned}$$

where the definition of $\mathbf{A}$-matrices is given in Appendix C.1.

Patch case: In case of one screen ($N = 1$) the relation is [21]

$$\begin{aligned}\boldsymbol{E}_{xy}|_U(\boldsymbol{k}_{mn}, z_1) =& \mathbf{B}_{11}(\boldsymbol{k}_{mn}) \cdot \eta_0 \boldsymbol{J}_S|_U(\boldsymbol{k}_{mn}, z_1) \\ & - A_U \mathbf{B}_{10}(\boldsymbol{k}_{00}) \cdot \boldsymbol{F}^+(\boldsymbol{k}_{00}, z_0)\delta_{m0}\delta_{n0}\end{aligned} \tag{C.11}$$

and for several screens *i.e.*, $N > 1$, the corresponding relations are, [21]

$$\begin{aligned}\boldsymbol{E}_{xy}|_U(\boldsymbol{k}_{mn}, z_j) =& \sum_{k=1}^{N} \mathbf{B}_{jk}(\boldsymbol{k}_{mn}) \cdot \eta_0 \boldsymbol{J}_S|_U(\boldsymbol{k}_{mn}, z_k) \\ & - A_U \mathbf{B}_{j0}(\boldsymbol{k}_{00}) \cdot \boldsymbol{F}^+(\boldsymbol{k}_{00}, z_0)\delta_{m0}\delta_{n0}, \qquad j = 1, 2, \ldots, N\end{aligned} \tag{C.12}$$

where the definition of **B**-matrices is given in Appendix C.1.

References

[1] J. D. Bjorken and S. D. Drell. *Relativistic Quantum Fields.* McGraw-Hill, New York, 1965.

[2] M. Born and E. Wolf. *Principles of Optics.* Cambridge University Press, Cambridge, U.K., seventh edition, 1999.

[3] B. Chambers. Optimum design of a salisbury screen radar absorber. *Proc. IEEE Lett.*, **30**(16), 1353–1354, 1994.

[4] B. Chambers and A. Tennant. Design of wideband Jaumann radar absorbers with optimum oblique incidence performance. *Electronics Letters*, **30**(18), 1530–1532, September 1994.

[5] W. C. Chew. *Waves and fields in inhomogeneous media.* IEEE Press, Piscataway, NJ, 1995.

[6] E. A. Coddington and R. Carlson. *Linear Ordinary Differential Equations.* SIAM, Philadelphia, 1997.

[7] R. E. Collin. *Foundations for Microwave Engineering.* McGraw-Hill, New York, second edition, 1992.

[8] F. Costa, A. Monorchio, and G. Manara. Analysis and design of ultra thin electromagnetic absorbers comprising resistively loaded high impedance surfaces. *IEEE Trans. Antennas Propagat.*, **58**(5), 1551–1558, 2010.

[9] T. A. Cwik and R. Mittra. Scattering from a periodic array of freestanding arbitrarily shaped perfectly conducting or resistive patches. *IEEE Trans. Antennas Propagat.*, **35**(11), 1226–1234, 1987.

[10] L. J. Du Toit. The design of Jauman absorbers. *IEEE Antennas and Propagation Magazine*, **36**(6), 17–25, 1994.

[11] L. J. Du Toit and J. H. Cloete. Electric screen Jauman absorber design algorithms. *IEEE Trans. Microwave Theory Tech.*, **44**(12 Part 1), 2238–2245, 1996.

[12] G. Eriksson. Efficient 3d simulation of thin conducting layers of arbitrary thickness. In *Proc. 2007 IEEE Intl Symp. Electromagentic Compability*, Honolulu, Hawaii, 8–13 July 2007.

[13] R. L. Fante, M. T. McCormack, T. D. Syst, and M. A. Wilmington. Reflection properties of the salisbury screen. *IEEE Trans. Antennas Propagat.*, **36**(10), 1443–1454, 1988.

[14] A. Ishimaru. *Electromagnetic Wave Propagation, Radiation, and Scattering.* Prentice-Hall, Inc., Englewood Cliffs, New Jersey, 1991.

[15] A. Karlsson. Approximate boundary conditions for thin structures. *IEEE Trans. Antennas Propagat.*, **57**(1), 144–148, 2009.

[16] A. Kazemzadeh and A. Karlsson. Capacitive circuit method for fast and efficient design of wideband radar absorber. *IEEE Trans. Antennas Propagat.*, **57**(8), 2307–2314, 2009.

[17] A. Kazemzadeh and A. Karlsson. Multilayered wideband absorbers for oblique angle of incidence. *IEEE Trans. Antennas Propagat.*, **58**(11), 3637–3646, 2010.

[18] G. Kiani, A. R. Weily, and K. P. Esselle. A novel absorb/transmit FSS for secure indoor outdoor wireless networks with reduced multipath fading. *IEEE Microwave and Wireless Components Letters*, **16**, 378–380, 2006.

[19] W. L. Ko and R. Mittra. Scattering by a truncated periodic array. *IEEE Trans. Antennas Propagat.*, **36**(4), 496–503, 1988.

[20] J. A. Kong. *Electromagnetic Wave Theory.* John Wiley & Sons, New York, 1986.

[21] G. Kristensson, S. Poulsen, and S. Rikte. Propagators and scattering of electromagnetic waves in planar bianisotropic slabs — an application to frequency selective structures. *Progress in Electromagnetics Research*, **48**, 1–25, 2004.

[22] I. V. Lindell, A. H. Sihvola, S. A. Tretyakov, and A. J. Viitanen. *Electromagnetic Waves in Chiral and Bi-isotropic Media.* Artech House, Boston, London, 1994.

[23] B. Munk. *Frequency Selective Surfaces: Theory and Design.* John Wiley & Sons, New York, 2000.

[24] B. Munk. *Metamaterials: Critique and Alternatives.* John Wiley & Sons, New York, 2009.

[25] B. A. Munk, P. Munk, and J. Pryor. On designing Jaumann and circuit analog absorbers (CA absorbers) for oblique angle of incidence. *IEEE Trans. Antennas Propagat.*, **55**(1), 186–193, January 2007.

[26] S. Poulsen. Scattering from frequency selective surfaces: A continuity condition for entire domain basis functions and an improved set of basis functions for crossed dipole. *IEE Proc.-H Microwaves, Antennas and Propagation*, **146**(3), 234–240, 1999.

[27] D. M. Pozar. *Microwave Engineering.* John Wiley & Sons, New York, 1998.

[28] S. Rikte, M. Andersson, and G. Kristensson. Homogenization of woven materials. *Archiv für Elektronik und Übertragungstechnik (AEÜ)*, **53**(5), 261–271, 1999.

[29] S. Rikte, G. Kristensson, and M. Andersson. Propagation in bianisotropic media—reflection and transmission. *IEE Proc. Microwaves, Antennas and Propagation*, **148**(1), 29–36, 2001.

[30] F. Sakran, Y. Neve-Oz, A. Ron, and M. Golosovsky. Absorbing frequency-selective-surface for the mm-wave range. *IEEE Trans. Antennas Propagat.*, **56**(8), 2649–2654, 2008.

[31] T. B. Senior. Approximate boundary conditions. *IEEE Trans. Antennas Propagat.*, **29**, 826–829, 1981.

[32] J. A. Stratton. *Electromagnetic Theory.* McGraw-Hill, New York, 1941.

[33] J. R. Wait. *Electromagnetic Waves in Stratified Media.* Pergamon, New York, second edition, 1970.